C. Quan, M. Kucukler, L. Gardner, Design of web-tapered steel I-section members by second-order inelastic analysis with strain limits, Eng. Struct. 224 (2020) 111242.

Design of web-tapered steel I-section members by second-order inelastic analysis with strain limits

Chunyan Quan[a*], Merih Kucukler[b], Leroy Gardner[a]

[a] *Department of Civil and Environmental Engineering, South Kensington Campus, Imperial College London, London SW7 2AZ, UK*

[b] *School of Engineering, University of Warwick, Coventry, CV4 7AL, UK*

* Corresponding author, Email: c.quan17@imperial.ac.uk

ABSTRACT

A consistent design approach, performed by second-order inelastic analysis using beam finite elements with strain limits, is proposed for web-tapered steel members. In the proposed design approach, a geometrically and materially nonlinear analysis with imperfections (GMNIA) of the tapered steel member is carried out and the ultimate strength of the member is signified by reaching either the strain limit defined according to the Continuous Strength Method (CSM) or the peak load factor, whichever occurs first. To consider the beneficial effect of strain gradients along the lengths of the members on local cross-section resistances, the strains are averaged over the local buckling half-wavelength. The accuracy of the proposed design approach is verified against results from nonlinear shell finite element modelling as well as a number of experiments on tapered members considering various taper ratios, loading conditions and member slenderness values. The proposed method provides more accurate and consistent

ultimate strength predictions than EN 1993-1-1 [1], because the following aspects, which are ignored in traditional design methods, are captured: (1) the interaction between cross-section elements for the consideration of local buckling, (2) the influence of local moment gradients on cross-section resistance, (3) the partial plastification of cross-sections and (4) strain hardening.

Keywords: Tapered members; Continuous Strength Method (CSM); Strain limits; Combined loading; Finite element modelling; Steel design; Buckling

1. INTRODUCTION

Web-tapered I-section members are commonly used in steel construction to enhance structural efficiency. Typically, cross-sections of greater depth are arranged to coincide with the regions of larger internal forces within the structure, such as at the eaves and apexes of steel portal frames, as shown in Fig. 1. In keeping with the design of structures comprising uniform members, the design of structures featuring tapered members also generally involves two steps: (i) the determination of the internal forces and moments within the structure through a structural analysis and (ii) the performance of a series of strength and stability checks on the individual members. The structural analysis is typically carried out using beam finite elements, which are not able to capture cross-section instabilities, i.e. local buckling is not accounted for and rotation capacities are unlimited. Hence, in current practice (e.g. EN 1993-1-1 [1]), cross-section instabilities are considered through the concept of cross-section classification, where cross-sections are placed into discrete classes that define the resistance and permitted analysis type, based on specified plate width-to-thickness ratios. This does however lead to artificial steps between different classes in the resistance predictions of steel members and systems. Tapered steel members are particularly prone to the shortcomings of the cross-section classification concept since their cross-sections continuously vary along the member length

and often fall into different classes, leading to abrupt changes in load carrying capacity depending upon the location of the most heavily utilised cross-section, which may change for different loading combinations and analysis types.

With the aim of overcoming the above drawbacks, an alternative design approach for tapered steel members performed using advanced analysis is presented in this paper. In the proposed approach, a second-order inelastic analysis i.e. a geometrically and materially nonlinear analysis with imperfections (GMNIA) of the tapered member is carried out using beam finite elements; the ultimate strength of the member is then determined based on either (i) the load factor corresponding to the attainment of the CSM (Continuous Strength Method [2]) strain limit within the member or (ii) the peak load factor, after which the load versus deformation response descends, whichever occurs first. The proposed approach exploits the benefits of advanced analysis such as its ability to (i) furnish very accurate ultimate strength predictions for individual members and systems, (ii) provide realistic structural failure modes and (iii) avoid the need for conducting member design checks, which can be particularly complex for tapered steel members [3-6]. The beneficial influence of strain gradients along the member lengths on the local cross-section strength is also allowed for by limiting averaged compressive strains over the local buckling half-wavelength rather than peak compressive strains at a specific cross-section using the CSM; this results in improved capacity predictions. The accuracy of the proposed design approach is verified against results from nonlinear shell finite element modelling as well as a number of experiments on tapered members with various taper ratios and member slenderness values. Furthermore, it is shown that the proposed design approach leads to a considerably more direct and practical way of designing tapered steel members relative to traditional design methods provided in design standards such as EN 1993-1-1 [1].

2. TRADITIONAL STEEL DESIGN APPROACH FOR TAPERED MEMBERS AND STRUCTURES

2.1 Shortcomings of current steel design approaches at member and overall structural levels

Structural steel design requires any limit state that is not captured in the structural analysis to be assessed separately through strength and stability checks. It suffices to state that in current practice, the most widely used structural analysis types are first-order (with or without amplification to simulate the effects of the deformed geometry at the overall frame level) or second-order elastic analysis. Since only the influence of overall geometric nonlinearity is considered in such an approach, subsequent individual member design checks, against the corresponding internal forces, are required. The ultimate resistances of the members are determined using member design equations that incorporate the effects of geometric imperfections and residual stresses. For regular, prismatic members, member design equations given in steel design specifications are generally well established, accurate and straightforward to apply. However, for tapered steel elements, member design equations provided in steel design specifications [1,7] are typically less well established and less accurate, as shown in Kucukler and Gardner [8,9], Marques et al. [10-13], and Tankova et al. [14-17]. Other design methods, developed specifically for tapered steel members [6,11,18-20] and yielding accurate resistance predictions also exist, but these methods are rather complex to apply, requiring a series of indirect steps, as outlined in [10-14,21-22], for the consideration of the tapered geometry and loading conditions on the structural response.

Design by second-order elastic analysis of tapered steel members using beam finite elements with equivalent member imperfections (i.e. GNIA) is also permitted in EN 1993-1-1 [1]. In this design approach, member out-of-straightness is explicitly modelled in the structural analysis using equivalent bow imperfection amplitudes that are greater than the maximum out-of-

straightness tolerances provided in the European execution standard EN 1090-2 [23] to allow for the influence of plasticity, residual stresses and geometric imperfections on member strengths. Thus, this approach removes the need to apply member design equations and only requires cross-section strength checks, resulting in very direct, though rather conservative [9], design approach for tapered steel members.

2.2 Shortcomings of current steel design approaches at cross-section level

In current design specifications, such as EN 1993-1-1 [1] and AISC 360-16 [24], the cross-section resistances of steel members are determined with reference to the cross-section classification concept. Based on the susceptibility to local buckling, a cross-section can be classified into one of four classes, namely Class 1 (plastic), Class 2 (compact), Class 3 (semi-compact) and Class 4 (slender). With reference to the typical moment-curvature relationships shown in Fig. 2, the following definitions are used in EN 1993-1-1 [1]: Class 1 cross-sections can attain their full plastic moment resistance M_{pl} and have sufficient rotation capacity ($R > 3$) for plastic design. Class 2 cross-sections can also reach their full plastic moment capacities M_{pl} but, because of their limited rotation capacity, may only be used in elastic design (i.e. no allowance is made for plastic redistribution). For Class 3 cross-sections, the elastic moment capacity M_{el} may be used as the bending resistance, while for Class 4 cross-sections, only the effective bending moment resistance M_{eff} may be used, which is calculated according to the effective width method given in EN 1993-1-5 [25]. Although it is straightforward to apply, there are a number of shortcomings with the cross-section classification concept.

- The first shortcoming is that classification is carried out only by considering the width-to-thickness ratio of the most critical plate element within the cross-section by conservatively assuming the web-to-flange junctions to provide simply-supported boundary conditions to the individual plates, thus ignoring the beneficial effect of element interaction [26].

- The second shortcoming relates to the lack of consideration for partial plasticity in Class 3 (semi-compact) cross-sections, though following recent research [27-29], the resulting artificial step in cross-section resistance has been overcome through the definition of an elasto-plastic bending resistance. This is due to be incorporated into the next revision to EN 1993-1-1.
- The third shortcoming is the lack of consideration given to material strain hardening in the determination of the resistance of stocky cross-sections, resulting in overly-conservative capacity predictions [30].
- The fourth shortcoming relates to the inconsistent allowance for the beneficial effect of moment gradients on element stability. This beneficial effect is accounted for when considering member stability, but is disregarded when evaluating local cross-sectional stability. This is despite numerous studies [31-36] showing improved bending resistances in beams tested in three-point bending (i.e. with a moment gradient) relative to those tested in four-point bending (i.e. with uniform moment in the central region).

3. DESIGN BY ADVANCED ANALYSIS USING BEAM ELEMENTS AND CSM STRAIN LIMITS

To overcome the shortcomings described above, as well as responding to the changing landscape with regards to the sophistication of available structural analysis software and computational power, Fieber et. al [37] proposed a new approach to structural steel design. The new design method involves: (i) using beam finite element models to perform an advanced inelastic analysis (i.e. GMNIA) and (ii) using either the load factor that corresponds to the attainment of the CSM strain limit or the peak load factor, whichever occurs first, to define the ultimate resistance of individual members or structures. The key aspects of the method and the use of the CSM strain limits in the advanced analysis of uniform members are briefly introduced below. Then, the extension of this design approach to tapered members is described.

3.1 Advanced analysis with CSM strain limits for uniform members

3.1.1 CSM *base curve, cross-section slenderness and material model*

The Continuous Strength Method (CSM) is a deformation-based approach to structural design that allows a continuous, rational and accurate treatment of material nonlinearity i.e. the partial spread of plasticity, strain hardening and inelastic force/moment redistribution, depending on the cross-section slenderness. The CSM was proposed by Gardner [2], and has been applied to the design of stainless steel [38,39], carbon steel [40,41] and aluminium alloy [42,43,44] structural members, as well as planar steel frames [45]. The CSM has two key features: (i) a base curve, described in the present sub-section, that defines the maximum strain ε_{csm} that a cross-section can experience prior to its failure; this is presented as a multiple of the yield strain ε_y and determined based on the cross-section slenderness $\bar{\lambda}_p$, defined below; (ii) an appropriate constitutive model describing the stress-strain response of the structural material, presented below. The CSM can be used as an alternative to the cross-section classification concept and provides a more consistent and continuous treatment of the influence of local instabilities on the ultimate resistances of cross-sections ranging from Class 1 to Class 4.

As shown in Fig. 3, the CSM base curve is split into two parts, and the transition point between non-slender and slender cross-sections is set at $\bar{\lambda}_p = 0.68$ [39]. For non-slender cross-sections ($\bar{\lambda}_p \leq 0.68$), the CSM strain limit is greater than or equal to the yield strain (i.e. $\varepsilon_{csm}/\varepsilon_y \geq 1$), given by Eq. (1), allowing the rational exploitation of the spread of plasticity and strain hardening. For slender cross-sections ($\bar{\lambda}_p > 0.68$), the CSM strain limit is less than the yield strain (i.e. $\varepsilon_{csm}/\varepsilon_y < 1$), as given by Eq. (2). In Eq. (1), there are two upper limits for $\varepsilon_{csm}/\varepsilon_y$. The first upper limit Ω is a project specific design parameter that defines the maximum permitted level of plastic deformation, for which the value of 15 is recommended, remaining within the EN 1993-1-1 [1] ductility requirements. The second upper limit $C_1\varepsilon_u/\varepsilon_y$ is established to avoid

over-predictions of material strengths [40], where C_1 is a coefficient related to the adopted material model, as described below.

$$\frac{\varepsilon_{csm}}{\varepsilon_y} = \frac{0.25}{\bar{\lambda}_p^{3.6}} \quad \text{but} \le \left(\Omega, \ \frac{C_1 \varepsilon_u}{\varepsilon_y} \right) \quad \text{for } \bar{\lambda}_p \le 0.68 \tag{1}$$

$$\frac{\varepsilon_{csm}}{\varepsilon_y} = \left(1 - \frac{0.222}{\bar{\lambda}_p^{1.05}} \right) \frac{1}{\bar{\lambda}_p^{1.05}} \quad \text{for } \bar{\lambda}_p > 0.68 \tag{2}$$

In Eqs. (1) and (2), the cross-section slenderness $\bar{\lambda}_p$ is determined from Eq. (3), where f_y is the material yielding stress and $\sigma_{cr,cs}$ is the elastic local buckling stress of the full cross-section which can be calculated numerically (e.g. through the finite strip software *CUFSM* [46]), or using the equations developed by Gardner et. al [26].

$$\bar{\lambda}_p = \sqrt{\frac{f_y}{\sigma_{cr,cs}}} \tag{3}$$

The second key feature of the CSM is the definition of an accurate and appropriate material model. In this study, the quad-linear stress-strain model for hot-rolled steels developed by Yun and Gardner **Error! Reference source not found.** was used for the studied tapered steel members, which were assumed to be formed by the welding of hot-rolled steel plates. The model has been shown to provide a very accurate representation of the stress-strain response of different steel grades, and is illustrated in Fig. 4. Unless otherwise indicated, grade S355 steel was used in all cases considered in this study, thus the three required parameters for the material model of **Error! Reference source not found.** were taken as the Young's modulus E = 210000 MPa, the yield stress f_y = 355 MPa and the ultimate stress f_u = 510 MPa. The stress-strain relationship over the full range is defined by Eq. (4), where the strain ε_{sh} at which strain hardening starts, the ultimate strain ε_u, and the strain hardening modulus E_{sh}, are defined by Eqs. (5)-(7) respectively.

$$f = \begin{cases} E\varepsilon & \text{for } \varepsilon \le \varepsilon_{\mathrm{y}} \\ f_{\mathrm{y}} & \text{for } \varepsilon_{\mathrm{y}} < \varepsilon \le \varepsilon_{\mathrm{sh}} \\ f_{\mathrm{y}} + E_{sh}\left(\varepsilon - \varepsilon_{\mathrm{sh}}\right) & \text{for } \varepsilon_{\mathrm{sh}} < \varepsilon \le C_1\varepsilon_{\mathrm{u}} \\ f_{C_1\varepsilon_{\mathrm{u}}} + \dfrac{f_{\mathrm{u}} - f_{C_1\varepsilon_{\mathrm{u}}}}{\varepsilon_{\mathrm{u}} - C_1\varepsilon_{\mathrm{u}}}\left(\varepsilon - C_1\varepsilon_{\mathrm{u}}\right) & \text{for } C_1\varepsilon_{\mathrm{u}} < \varepsilon \le \varepsilon_{\mathrm{u}} \end{cases} \quad (4)$$

$$\varepsilon_{\mathrm{sh}} = 0.1\frac{f_{\mathrm{y}}}{f_{\mathrm{u}}} - 0.055 \qquad \text{but } 0.015 \le \varepsilon_{\mathrm{sh}} \le 0.03 \quad (5)$$

$$\varepsilon_{\mathrm{u}} = 0.6\left(1 - \frac{f_{\mathrm{y}}}{f_{\mathrm{u}}}\right) \qquad \text{but } \varepsilon_{\mathrm{u}} \ge 0.06 \quad (6)$$

$$E_{\mathrm{sh}} = \frac{f_{\mathrm{u}} - f_{\mathrm{y}}}{C_2\varepsilon_{\mathrm{u}} - \varepsilon_{\mathrm{sh}}} \quad (7)$$

Finally, in the adopted material model, the constants C_1 and C_2 are given by Eqs. (8) and (9) respectively.

$$C_1 = \frac{\varepsilon_{\mathrm{sh}} + 0.25\left(\varepsilon_{\mathrm{u}} - \varepsilon_{\mathrm{sh}}\right)}{\varepsilon_{\mathrm{u}}} \quad (8)$$

$$C_2 = \frac{\varepsilon_{\mathrm{sh}} + 0.4\left(\varepsilon_{\mathrm{u}} - \varepsilon_{\mathrm{sh}}\right)}{\varepsilon_{\mathrm{u}}} \quad (9)$$

3.1.2 Concept

Through GMNIA with beam elements, member instabilities can be captured directly, but local instabilities cannot. Thus, in [37], it has been recommended that the CSM strain limits are adopted to account for local buckling effects; the maximum compressive strains are checked against the corresponding CSM strain limits at all cross-sections in the structure at each load increment. The load factor at failure is defined as either (i) the load factor at which the CSM strain limit is attained or (ii) the peak load factor obtained from the advanced analysis, whichever occurs first.

3.1.3 Strain averaging approach

In previous research [31-36], it has been observed that laterally restrained steel beams subjected to moment gradients exhibit greater cross-section resistances than the same beams under uniform bending. This has been ascribed to the beneficial effects of strain gradients along

member lengths on the local stability of cross-sections [37,48], i.e. the critical cross-section receives support from the adjacent less heavily loaded cross-sections. It was shown in [37] that this effect could be accurately captured by limiting averaged rather than peak compressive strains to the CSM strain limit. The length of member of which to average the strains was taken as the elastic local buckling half-wave length $L_{b,cs}$ that can be obtained numerically e.g. using the finite strip method software *CUFSM* [46] or through the expressions presented in [49].

3.2 Extension to tapered members

3.2.1 Procedure for application of CSM strain limits in GMNIA of tapered members

In the proposed design method, the first step is to use beam element models to perform GMNIA of the tapered member. In this study, the finite element analysis package Abaqus [50] was used to carry out the GMNIA simulations. A common method for analysing tapered members is to divide them into a sufficient number of prismatic segments [22]; at least twenty is recommended [51]. Although the influence of the inclined flanges of the tapered members on their internal stress distributions is neglected in this approach, it has been established that, for tapering angles typically encountered in practice (<15°), this influence is negligible and, hence the in-plane behaviour of tapered steel members can be accurately modelled using a series of prismatic beam elements [10]. Thus, in the implementation of the proposed design method in this paper, the analysed tapered members, all of which had a taper angle of less than 15°, were modelled as stepped members with prismatic cross-sections for each element, as shown in Fig. 5. The cross-section properties of each element were taken equal to the corresponding cross-section properties at the midspan of the element. The shear deformable prismatic Timoshenko beam element for open cross-sections, referred to as B31OS in Abaqus [50], was adopted. To accurately capture the spread of plasticity, each web and flange plate was discretised into 33 section points along the width. To enable the correct application of the strain averaging approach, used to consider the beneficial influence of strain gradients along the member lengths,

the element sizes were taken as less than or equal to the shortest local buckling half-wavelength $L_{b,cs}$ determined for all cross-sections within the considered tapered member, in accordance with the recommendations of [37].

In the application of the proposed method, the quad-linear material model introduced in the Section 3.1.1 was employed, adopting the engineering stress-strain curve since the cross-sectional areas of the beam elements remained constant throughout the analyses. Since the explicit modelling of residual stress in the design of steel structures with advanced analysis can be somewhat impractical, the use of the equivalent geometric imperfections provided in prEN 1993-1-1 [52], as developed by Lindner [53], to consider the combined influence of both geometric imperfections and residual stresses, is recommended in the implementation of the proposed design method. Since GMNIA explicitly considers the development and spread plasticity, the equivalent imperfection magnitudes developed for use with elastic cross-section checks [52,53] were adopted to avoid double-counting the detrimental effect of plasticity. Further discussion on this issue and recommended equivalent bow imperfection magnitudes for use specifically in GMNIA of prismatic members are presented in [54]. The geometric imperfections were assigned to the beam element models in the shape of the lowest global buckling modes from prior Linear Buckling Analyses (LBA). The investigated tapered members were pin-ended and laterally restrained in all the considered cases to suppress lateral-torsional buckling effects.

Following the beam element analysis of the tapered member, the ultimate capacity can be determined according to the proposed procedure illustrated in Fig. 6.

- First, based on the first-order internal force distribution, the local buckling stress of the full cross-sections of all prismatic beam elements along the member length $\sigma_{cr,cs,m}$ (where m denotes the number of the beam element) is obtained [26,46].

- Then, using Eq. (3), the corresponding cross-section slendernesses $\bar{\lambda}_{p,m}$ along the member length are determined.
- According to the value of $\bar{\lambda}_{p,m}$, the strain limit for each element $\varepsilon_{csm,m}$ is obtained from the base curve.
- If the strain averaging approach is applied, the local buckling half-wavelength of each cross-section $L_{b,cs,m}$ needs to be calculated, using *CUFSM* [46] or the expressions provided in [49]; the average strain for each element $\varepsilon_{Ed,av,m}$ is taken as the average value of strains $\varepsilon_{Ed,m}$ over the corresponding local buckling half-wavelength $L_{b,cs,m}$, as shown in Fig. 7. Note that only beam elements fully located within $L_{b,cs,m}$ are considered in the strain averaging approach. It should be emphasised that, unlike in prismatic members, strain gradients occur along the lengths of tapered members even under uniform loading.
- Finally, it is necessary to determine (i) the load increment p at which the average strain at any cross-section m_0 attains the corresponding CSM strain limit, i.e. $\varepsilon_{Ed,av,m_0,p} \geq \varepsilon_{csm,m_0}$ and (ii) the load increment j (if any) at which the peak load factor is reached. If j < p, the member is assumed to have failed primarily due to global instability, and the ultimate load carrying capacity α_u is taken as the peak load factor from the GMNIA α_{peak}. On the other hand, if j > p, the tapered member is assumed to have failed due to reaching the cross-section capacity, and the load factor at which the strain limit is attained is adopted as the ultimate member resistance α_u.

3.2.2 Illustrative examples

The benefits of the proposed design method can be best demonstrated through an illustrative example. Fig. 8 presents the normalised moment-strain response from a beam finite element (FE) model of a tapered member under uniform bending. In the figure, the end bending moment M, is normalised by the full plastic moment capacity at the shallow end of the tapered member $M_{pl,s}$; the strain plotted is the average maximum compressive strain over the local buckling

half-wavelength at the critical beam element (m_0) ε_{Ed,av,m_0}, normalised by the yield strain ε_y. In the beam element GMNIA of this tapered member, no peak load factor was reached, and the end bending moment continuously increased. Thus, this member was deemed to have failed when the CSM strain limit was reached at the critical cross-section. The CSM strain limit at the critical cross-section ε_{csm,m_0} was equal to $7.89\varepsilon_y$; when ε_{Ed,av,m_0} reached $\varepsilon_{csm,m_0} = 7.89\varepsilon_y$, the analysis was terminated and the bending moment capacity of the beam was calculated as $M_{u,prop} = 1.053M_{pl,s}$. The corresponding benchmark shell FE model of the same member (whose development and validation is described in detail in Section 4) reached a peak bending moment of $M_{u,shell} = 1.112M_{pl,s}$, following the occurrence of local buckling in the compression flange at the critical cross-section; of course local buckling is explicitly captured in the shell FE model and hence application of the CSM strain limit is neither appropriate nor required. Compared to the capacity obtained from the benchmark shell FE model, the prediction obtained using the proposed design method of beam element GMNIA with strain limits is only 5% lower. On the other hand, the ultimate load carrying capacity of the member according to EN 1993-1-1 [1] (using GNIA plus cross-section checks) is signified by reaching the plastic moment capacity $M_{pl,s}$ at the shallow end of the member, which is approximately 10% below the shell FE result. Note that in this example, and all the considered cases in this study, the strain outputs, elastic local buckling stresses and corresponding defined CSM strain limits, are all compatibly determined at, or calculated based on, the centreline of the wall thickness, as recommended in [37].

A further illustrative example of the proposed method applied to a tapered column is presented in Fig. 9, which shows (i) the variation of the CSM strain limit ε_{csm} (because of the changing geometry), the total compressive strain $\varepsilon_{Ed,I+II}$, the first order strain $\varepsilon_{Ed,I}$ and the second order strain $\varepsilon_{Ed,II}$ along the member length at the load increment when the CSM strain limit is first reached, and (ii) the corresponding variation in the strain utilisation ratio along the member

length. The taper ratio γ (i.e. the ratio of the deep-section height h_d to the shallow-section height h_s) of this tapered column is equal to 5, and the major axis normalised member slenderness $\bar{\lambda}_y$, which is defined as the square root of the axial yield load of the shallow end cross-section $N_{pl,s}$ divided by the elastic buckling load N_{cr} is equal to 0.8 (i.e. $\bar{\lambda}_y = \sqrt{N_{pl,s} / N_{cr}} = 0.8$). As can be seen from Fig. 9, in the proposed design method, (i) the second order effects can be accurately and directly captured through the GMNIA, (ii) the critical cross-section can be determined in a straightforward manner and (iii) the contribution of the first order and second order effects on the strain utilisation can be clearly observed. Considering the strain distribution at the ultimate state, it is even possible to optimise the geometry of a tapered member in terms of material use by aiming to achieve a uniform strain utilisation ratio along the member length.

4. BENCHMARK SHELL FINITE ELEMENT MODELLING

4.1 Modelling approach

The accuracy of the proposed design approach is verified for a large number of tapered members against results obtained from benchmark shell finite element models. The finite element analysis software Abaqus [50] was used to create the shell finite element models in this study. The element type S4R, a four-noded shell element taking into account transverse shear deformation and finite membrane strains with reduced integration and a large-strain formulation, which has been successfully employed in previous study for similar applications [9,37,55,56], was used to create the models. All cross-sections were subdivided into 16 elements along the flange width and the web depth. The element number along the longitudinal axis of a tapered member was defined such that the element aspect ratio at the midspan cross-section was close to unity. The Simpson integration method was used, and five integration points were employed through the thickness of the shell elements [50].

The quad-linear stress-strain model developed by Yun and Gardner **Error! Reference source not found.** for hot-rolled steel was used in the models. The Poisson's ratio was taken as v = 0.3 in the elastic range and v = 0.5 in the plastic range. As required by Abaqus [50], for shell finite element models, the engineering stress-strain relationships were transformed into the true stress-strain relationships.

Beam multi-point constraints were used to couple the web and two flange plates making up the investigated members. To avoid overlapping of the web and flange plates, the web nodes were offset by half the flange thickness at the top and bottom, in line with the approach adopted in [9,57,58]. Since this study focuses only on the in-plane behaviour of tapered steel members, lateral-torsional buckling effects were suppressed by laterally restraining the models at the web-to-flange junctions along their lengths. Boundary conditions and concentrated forces and moments were applied at the member ends by defining coupling constraint relationships. The ECCS [59] residual stress pattern illustrated in Fig. 10, which is recommended for steel members fabricated by the welding of individual steel plates [9,60], was adopted in the finite element models. Global geometric imperfections were assigned to the models in the shape of the lowest global buckling modes. Unless otherwise indicated, the magnitudes of the global geometric imperfections were taken as l/1000, where l is the member length. As shown in Fig. 11, local imperfections were applied to the shell finite element models by adopting a series of sinusoidal subpanel imperfections complying with the recommendations provided in Annex C of EN 1993-1-5 [25]. For the cases where the web plate was more susceptible to local buckling than the flange plates, i.e. when $\sigma_{cr,w} < \sigma_{cr,f}$ (where $\sigma_{cr,w}$ and $\sigma_{cr,f}$ are the elastic local buckling stresses of the isolated web and flange plates respectively with simply-supported boundary conditions along the adjoined edges), the magnitudes of the local web imperfection was taken as 1/200 of the web height h_w (i.e. h_w/200). Similarly, for the cases where the flange plates were more susceptible to local buckling than the web plate, the magnitude of the local flange

imperfection was taken as 1/100 of the flange widths b (i.e. b/100). The local imperfection magnitudes of the non-critical plate elements were defined such that the web-to-flange junctions remained at 90°. The half-wavelengths $L_{b,cs}$ of the local imperfections were obtained from the expressions in [49]. Since tapered members have variable cross-section depths along their lengths, there are different local buckling half-wavelengths for each cross-section; to reflect this, the local buckling half-wavelengths $L_{b,cs}$ used to represent the local imperfections were also varied along the member length, as explained in Fig. 12. Starting at the deep end of the member, the local buckling half-wavelengths $L_{b,cs,n}$ were calculated at sequential cross-sections (separated by the distances $L_{b,cs,n}$) until the shallow end of the member was reached. In the event that the sum of the local buckling half-wavelengths (i.e. $\sum L_{b,cs,n}$) was not exactly equal to the member length L, which was generally the case, an integer number of half-waves was ensured by uniformly stretching or contracting the $L_{b,cs,n}$ values by a factor x, such that the ratio $L/\sum xL_{b,cs,n}$ was equal to unity – see Fig. 12.

4.2 Validation of shell FE models

The shell FE models were validated against the results from eighteen tapered member experiments collected from the literature. In the experimental studies [5,16,61,62] considered for the validation of the shell FE models developed herein, tapered members with different taper ratios were tested, including columns [16], beams under different bending moment gradients [61] and beam-columns [5,62] which had either (i) no intermediate lateral restraint (NR), (ii) lateral restraints only (LR) or (iii) both lateral and torsional restraints (TR) between the end supports. Although the focus of the present study is the in-plane behaviour and design of tapered steel members, a few experiments on tapered members without out-of-plane restraints and susceptible to lateral-torsional buckling were also included in the validation study; in these cases, the boundary conditions applied in the FE models mirrored those adopted in the tests. In the validation study, the measured magnitudes of the global geometric imperfections

from the considered experiments were applied to the FE models in the shape of their lowest global elastic buckling modes. For the cases where the geometric imperfection magnitudes were not reported, the lowest global elastic buckling modes were scaled to 1/1000 of the member lengths. A summary of the results of the validation study, including the mean, coefficient of variation (CoV), minimum and maximum values of the ratios of the ultimate load carrying capacities determined using the shell FE models to those obtained from the experiments ($\alpha_{u,shell}/\alpha_{u,test}$), are given in Table 1. As can be seen from the table, the shell FE models are able to provide ultimate strength predictions very close to those observed in the physical experiments for tapered columns, beams and beam-columns.

Fig. 13 shows experimental and numerical load-displacement curves for the tapered column specimen C1 tested in [16], while Fig. 14 shows experimental and numerical moment-rotation curves for the tapered beam-column specimens with lateral and torsional restraints (C1-8-TR) and without lateral restraints (C2-6-NR) tested in [62]. As can be seen from the figures, the load-deformation paths obtained from the shell finite element models developed in this study closely follow the corresponding experimentally determined paths; this indicates that the developed models are able to replicate the observed structural response of tapered members and can be used to generate benchmark data to evaluate the accuracy and safety of the proposed design approach in this paper.

5. APPLICATION OF PROPOSED DESIGN METHOD TO MEMBERS UNDER PURE COMPRESSION, UNIFORM BENDING AND COMBINED COMPRESSION AND UNIFORM BENDING

In this section, the accuracy of the proposed design method of advanced analysis with strain limits, implemented in beam finite element models, is assessed against the results from the benchmark shell finite element models for tapered members subjected to compression, uniform

bending and combined compression and uniform bending. The accuracy of the traditional design method presented in Eurocode 3 [1] for tapered members, i.e. second-order elastic analysis with equivalent imperfections (GNIA) plus cross-section checks, is also presented in order to highlight the benefits brought about by the proposed design approach. It should be noted though that even greater benefits arise when performing system-level, rather than member-level, design.

As listed in Table 2, the investigations carried out in this section cover a range of normalised slenderness values $\bar{\lambda}_y = \sqrt{N_{pl,s} / N_{cr}}$ = 0.2, 0.5, 0.8, 1.2, 1.5 and a range of taper ratios $\gamma = h_d/h_s$ = 1, 2, 3, 4, 5. A series of different shallow end cross-section geometries were also considered – the employed cross-section geometries were those of European HEM 100, HEM 120, HEB 140, IPE 160, HEM 180, HEB 200, HEB 220, HEB 240 profiles, but without the presence of the fillet radii. Note that the maximum cross-section slenderness $\bar{\lambda}_p$ along the length of the tapered members did not exceed 1.5.

5.1 Tapered steel members subjected to pure compression

Fig. 15 (a) and Table 2 show that the ultimate capacities of 200 the tapered columns (5 values of $\bar{\lambda}_y$ × 5 taper ratios × 8 cross-sections) predicted using the proposed design method generally agree well with those obtained from the benchmark shell element models. With increasing taper ratios, the accuracy of the ultimate resistances obtained using the proposed design method decreases slightly. However, even for the tapered columns with a taper ratio of γ = 5 (which are generally rarely used in practice), the average value of the ratios of the resistance predictions determined using the proposed design method to those obtained from the benchmark shell FE models, i.e. $N_{u,prop}/N_{u,shell}$, is equal to 0.894, indicating that even for very large taper ratios, the proposed method provides accurate and safe-sided ultimate strength predictions. In contrast, the predictions obtained from Eurocode 3 (GNIA + cross-section

checks) are more conservative and scattered, highlighting the significantly more accurate and consistent ultimate strength predictions achieved when the proposed method is used for the design of tapered columns.

5.2 Tapered steel members subjected to pure uniform bending

Fig. 15 (b) and Table 2 present comparisons of the ultimate bending capacities of the considered 200 tapered beams obtained using the proposed design method and EN 1993-1-1 [1] against the results from their benchmark shell element model counterparts. According to the proposed design method, all the tapered beams failed by reaching their CSM strain limits. As can be seen from Fig. 15 (b), the predicted ultimate bending moment capacities are generally very accurate, though in some cases, the predictions are somewhat lower than those obtained from the shell FE models, e.g. $M_{u,prop}/M_{u,shell} \approx 0.8$. These conservative predictions occurred for tapered members with very stocky ($\bar{\lambda}_{p,cr} \lesssim 0.32$) critical cross-sections (i.e. the cross-sections where the strain limit was attained), as shown in Fig. 16. However, if the upper strain limit $\varepsilon_{csm}/\varepsilon_y$ adopted for these members is relaxed from 15 to 30 (i.e. if additional strain hardening is allowed for these members), higher and thus more accurate bending moment resistances can be attained. Hence, although to prevent excessive deformations, the upper strain limit of $15\varepsilon_y$ is usually recommended, if higher strains can be tolerated at the ultimate limit state, the upper limit of $30\varepsilon_y$ can be adopted to improve accuracy. In contrast with the proposed design approach, the EN 1993-1-1 [1] approach (in which moments cannot exceed the plastic moment capacity) is generally overly-conservative, thus indicating that the proposed design approach leads to considerably more accurate ultimate strength predictions for tapered members under bending.

The high accuracy of the proposed design method is achieved partly through the adoption of the strain averaging approach, which allows for the beneficial effect of local strain gradients along the member length on the resistance of cross-sections, as explained in Section 3.1.4. This

is illustrated in Fig. 17, which shows the variation of the CSM strain limit ε_{csm}, the maximum longitudinal compressive strain ε_{Ed} (at the mid-thickness of the compression flange) and the average maximum longitudinal compressive strain over the local buckling half-wavelength $\varepsilon_{Ed,av}$ at the load increment when the CSM strain limit is first reached. According to EN 1993-1-1 [1], the critical cross-section of this tapered beam is at the shallow end, which falls into the Class 1 category. Thus, the ultimate resistance of this beam arises when the bending moment at the shallow end of the member reaches the plastic moment resistance of the shallow end cross-section i.e. $M_{u,EC3}/M_{pl,s}$ = 1.000; this is however a significant underestimation of the ultimate strength of the beam, determined as $M_{u,shell}/M_{pl,s}$ = 1.322 from the benchmark shell finite element model. Using the proposed design method, but without employing strain averaging, the ultimate resistance of the beam is calculated as $M_{u,prop}/M_{pl,s}$ = 1.010; this corresponds to the point at which the CSM strain limit is reached at the shallow end cross-section, which has a cross-section slenderness equal to $\bar{\lambda}_p$ = 0.39. On the other hand, if the strain averaging approach is applied in the implementation of the proposed design method by limiting $\varepsilon_{Ed,av}$ over $L_{b,cs}$ (rather than ε_{Ed}) to ε_{csm}, the beneficial influence of the strain gradient along the beam length is considered; this results in an ultimate design resistance of the beam of $M_{u,prop}/M_{pl,s}$ = 1.184, which represents an improvement of 15% relative to the ultimate resistance determined according to EN 1993-1-1 [1].

5.3 Tapered steel members subjected to combined compression and uniform bending

In this subsection, the accuracy of the proposed design method of advanced analysis with strain limits implemented by beam elements is assessed for 2000 tapered members (5 $\bar{\lambda}_y$ × 5 γ × 8 cross-sections × 10 N to M ratios) under uniform bending plus axial compression. As shown in Fig. 18 (a) and Table 2, the proposed method is able to provide very accurate capacity predictions with a mean value of 0.950 and a CoV of 7.4% for the ratios of the ultimate load

carrying capacities determined by the proposed method to those obtained from the benchmark shell FE models. On the other hand, EN 1993-1-1 [1] yields less accurate and more scattered predictions with a mean value of 0.888 and a CoV of 11.2%. Note that EN 1993-1-1 [1] is particularly conservative for tapered members with large taper ratios γ, as shown in Fig. 18 (b). Comparing Fig. 18 (a) and Fig. 18 (b) shows that the proposed method provides more reliable ultimate strength predictions relative to EN 1993-1-1 [1], where the majority of the predictions obtained through the proposed design approach are very close to those obtained from the benchmark shell finite element models.

Normalised moment-axial force interaction diagrams for a series of tapered members with HEB 140 and HEB 220 sections at the shallow ends and subjected to combined compression and major axis bending are shown in Fig. 19. According to EN 1993-1-1 [1], the critical cross-sections (i.e. the cross-sections where the cross-section resistance is attained) of these tapered members all fall into the Class 1 category, and thus the ultimate resistances of these members were determined using the linear plastic bending moment-axial force (M-N) interaction equation provided in the standard and the corresponding imperfection amplitudes provided in prEN 1993-1-1 [52] for a linear plastic cross-section strength check. The EN 1993-1-1 [1] strength predictions for these members are rather conservative. By contrast, the proposed design method is able to accurately capture the behaviour observed in the benchmark shell finite element models. According to the proposed design approach, mirroring the shell finite element models, for the short members and for the members where bending is dominant, the load carrying capacities are governed by reaching the CSM strain limit at the critical cross-sections, while for the longer members, where global instability effects are dominant, the ultimate capacities correspond to the peak load factor obtained from the beam element analyses.

Similar observations can also be made in Fig. 20, which presents comparisons between the ratios of the ultimate capacities determined using the proposed design method and EN 1993-1-1 [1] to those determined from the benchmark shell finite element models ($\alpha_u/\alpha_{u,shell}$) versus the cross-section slenderness at the critical location $\bar{\lambda}_{p,cr}$ for all the analysed tapered members. The critical location refers to the cross-section where the strain limit is attained or the shallow end cross-section when the ultimate capacity is predicted by the peak load factor. For the tapered members with critical cross-sections of intermediate slenderness ($0.32 \lesssim \bar{\lambda}_{p,cr} \lesssim 0.5$), the improved accuracy and enhanced resistances achieved using the proposed design method relative to EN 1993-1-1 [1] arise due to the rational exploitation of the spread of plasticity and the allowance for local moment gradients through strain averaging. For the tapered members with critical cross-sections of stocky proportions ($\bar{\lambda}_{p,cr} \lesssim 0.32$), the proposed design method also allows for material strain hardening, which leads to further improvements in the accuracy of the resistance predictions. For the members with very stocky critical cross-sections, if the upper strain limit is increased from $15\varepsilon_y$ to $30\varepsilon_y$, the accuracy of the proposed design method improves even further, as shown in Fig. 21. For the tapered members with slender critical cross-sections ($\bar{\lambda}_{p,cr} \geq 0.68$), the ultimate resistances predicted by the proposed design method are close to those obtained from EN 1993-1-1 [1], as shown in Fig. 20. However, note that the cumbersome process of the determination of the effective section properties for Class 4 cross-sections is not required in the application of the proposed design method.

Similar to EN 1993-1-1 [1], in which cross-section classification is typically based on cross-section stress distributions determined from a first order elastic analysis of a steel member, in this study, cross-section slendernesses $\bar{\lambda}_p = \sqrt{f_y / \sigma_{cr,cs}}$ and hence the corresponding CSM strain limits ε_{csm} are also calculated using local buckling stresses $\sigma_{cr,cs}$ corresponding to the stress distribution from a first order elastic analysis. Typically, CSM strain limits ε_{csm} based on cross-

section stress distributions determined from the GMNIA of members will result in an increase in deformation capacity, because the ratio of bending moment to axial force generally increase during the analysis as second order effects become increasingly dominant. This results in a more favourable stress distribution for local buckling, with increasing values of $\sigma_{cr,cs}$ leading to lower values of slenderness $\bar{\lambda}_p$ and hence increased deformation capacities. This is illustrated in Fig. 22, which shows that higher strain limits and improved accuracy can be achieved when the stress distribution associated with the deformed geometry (i.e. allowing for second order effects) is considered in the determination in $\sigma_{cr,cs}$ (and hence $\bar{\lambda}_p$ and $\varepsilon_{csm}/\varepsilon_y$), but at the expense of greater calculation effort. Note that the slightly unconservative results in Fig.21 are not affected by this issue, since these members are either relatively short or their critical cross-sections are located near to one of the ends of the members; in both cases, second order effects are not significant.

6. APPLICATION OF PROPOSED DESIGN METHOD TO MEMBERS UNDER NON-UNIFORM BENDING AND COMBINED COMPRESSION AND NON-UNIFORM BENDING

In this section, the proposed design method of advanced analysis with strain limits is applied to 1680 tapered members subjected to different shapes of bending moment diagrams along their lengths, with or without axial compression. As summarised in Table 3, the following parameters were varied in the study: (i) the ratio of applied compression to bending moment, (ii) the ratio ψ of the bending moment applied at the shallow end of the member M_s to that applied at the deep end M_d, with values of $\psi = M_s/M_d$ = -1, -0.5, 0 and 0.5, as shown in Fig. 23, (iii) the normalised member slenderness with values of $\bar{\lambda}_y$ = 0.5, 1 and 1.5, (iv) the taper ratio with values of γ = 1, 2, 3, 4 and 5 and (v) the cross-section profile at the shallow end of the tapered members, whose geometric properties were taken as the same as those of European

HEM 100, HEM 120, HEB 140, IPE 160, HEM 180, HEB 220 and HEB 240 cross-sections. For all the considered tapered members, the maximum cross-section slenderness $\bar{\lambda}_p$ along the length did not exceed 1.5.

The presence of a moment gradient implicitly means that a tapered member is also subjected to shear forces, and high shear forces may negatively influence the ultimate load carrying capacities of tapered steel members. To allow for this effect, in this study, the approach proposed in [37] was adopted; thus, when the design shear force V_{Ed} exceeded half of the plastic shear force capacity of the cross-section $V_{pl,Rd}$, the interaction between bending and shear was accounted for through a reduction factor ρ_{csm} applied to the CSM strain limit, as described in [37]. The expression for the determination of the reduction factor ρ_{csm} is given by Eq. (10). The CSM shear reduction factor ρ_{csm} utilises the shear reduction factor defined in EN 1993-1-1 [1] ρ, which is given by Eq. (11). Note that separate cross-section shear capacity and shear buckling checks are still required in the application of the proposed design method which can be carried out using the provisions of EN 1993-1-1 [1] and EN 1993-1-5 [25].

$$\rho_{csm} = \begin{cases} 1 & \text{for } V_{Ed} \le 0.5V_{pl,Rd} \\ \dfrac{0.5}{0.5+\rho} & \text{for } V_{Ed} > 0.5V_{pl,Rd} \end{cases} \tag{10}$$

$$\rho = \left(\frac{2V_{Ed}}{V_{pl,Rd}} - 1 \right)^2 \tag{11}$$

Frequency distributions of the ratios of the ultimate resistances predicted by the proposed design method and EN 1993-1-1 [1] to those determined from the benchmark shell finite element models are shown in Fig. 24. As can be seen from the figure, the proposed design method provides accurate and generally safe-sided resistance predictions for tapered members subjected to compression plus non-uniform bending. As presented in Fig. 24 and Table 3, relative to EN 1993-1-1 [1] (i.e. GNIA plus cross-section checks), the proposed design method

offers an average of 4% to 9% improvement in accuracy, depending on the loading case considered, as well as a consistent reduction in the scatter of the predictions. As shown in Fig. 25, the traditional method presented in EN 1993-1-1 [1] becomes increasingly conservative for larger taper ratios γ.

Normalised bending moment-axial force interaction diagrams for a series of tapered members subjected to compression plus non-uniform bending are shown in Fig. 26. In the figure, $M_{u,s}$ and $M_{u,d}$ are the ultimate bending moments at the shallow and deep ends of the tapered members respectively, and $M_{pl,s}$ and $M_{pl,d}$ are the plastic bending moment resistances of the cross-sections at the shallow and deep ends. According to EN 1993-1-1 [1], the critical cross-sections (i.e. the cross-sections where the internal bending moment and axial compression reached the ultimate cross-section resistance) of these members fall into the Class 1 category; hence, the ultimate load carrying capacities of these tapered members are determined using the linear plastic bending moment-axial force (M-N) interaction equations provided in EN 1993-1-1 [1]. Similar to the observations made in Section 5 for tapered members under compression plus uniform bending, the design method presented in EN 1993-1-1 [1], i.e. GNIA plus cross-section checks, is rather conservative for tapered members under compression plus non-uniform bending. On the other hand, the proposed design method offers more accurate but still generally safe-sided strength predictions.

Similar observations can also be made based on Fig. 27, which presents comparisons between the ratios of the ultimate capacities predicted using the proposed design method and EN 1993-1-1 [1] to those determined from the benchmark shell FE models ($\alpha_u/\alpha_{u,shell}$) versus the cross-section slenderness at the critical location $\bar{\lambda}_{p,cr}$ for all the analysed tapered members. The critical location refers to the cross-section where the strain limit is attained or the shallow end cross-section when the ultimate capacity is predicted by the peak load factor. It can be seen

from Fig. 27 that, similar to the observations made in Section 5, for the tapered members with critical cross-sections of intermediate slenderness ($0.32 \lesssim \bar{\lambda}_{\mathrm{p,cr}} \lesssim 0.5$), the improved accuracy and enhanced resistances achieved using the proposed design method relative to EN 1993-1-1 [1] arise due to the rational exploitation of the spread of plasticity and the allowance for local moment gradients through strain averaging. For the tapered members with critical cross-sections of stocky proportions ($\bar{\lambda}_{\mathrm{p,cr}} \lesssim 0.32$), the proposed design method also allows for strain hardening, which results in further improvements in the accuracy of the resistance predictions. For the members with very stocky critical cross-sections, if the upper strain limit is increased from $15\varepsilon_{\mathrm{y}}$ to $30\varepsilon_{\mathrm{y}}$, the accuracy of the proposed design method improves even further, as shown in Fig. 28. For the tapered members with slender critical cross-sections ($\bar{\lambda}_{\mathrm{p,cr}} \geq 0.68$), the ultimate resistances predicted by the proposed design method are close to those obtained from EN 1993-1-1 [1].

In addition to the verification of the accuracy of the proposed design approach against the results from the benchmark shell finite element models, its accuracy is also assessed against the results obtained from available experiments on tapered members under uniform and non-uniform bending reported in the literature [5,16,61,62], as shown in Table 1. As can be seen from the table, the ultimate strengths determined using the proposed design method are somewhat conservative, but substantially more accurate and consistent than EN 1993-1-1 [1]. The conservatism is attributed to the use of the lowest eigenmode affine geometric imperfections with equivalent imperfection magnitudes in the proposed design method, both of which are more severe than the actual measured imperfections in the test specimens.

7. CONCLUSIONS

A consistent design method for tapered steel members performed by advanced inelastic analysis using beam finite elements with CSM strain limits has been put forward in this paper.

The proposed design method was applied to a total of 2000 tapered members subjected to compression, uniform bending and combined compression and uniform bending, and also to a total of 1680 tapered members under non-uniform bending and combined axial compression and non-uniform bending. Various taper ratios, geometrical properties, loading conditions and member slenderness values were considered. The accuracy of the proposed design method was extensively verified against results from nonlinear shell finite element modelling as well as a number of experiments on tapered members. It was shown that the proposed method provides consistently more accurate ultimate strength predictions relative to the traditional design method provided in EN 1993-1-1 [1] for the design of tapered steel members owing to (i) taking account of the interaction between cross-section elements in the determination of local slenderness, (ii) allowing for strain hardening in stocky cross-sections, (iii) exploiting partial plastification in cross-sections and (iv) considering the beneficial effects of strain gradients along the member lengths. The proposed method also precludes the need for cross-section classification, the cumbersome process of determining effective section properties for Class 4 cross-sections, individual member buckling design checks and the calculation of effective lengths in the determination of the ultimate strengths of tapered steel members. Future research will focus on extension of the proposed design method to steel frames made of tapered steel members and to uniform and tapered steel members susceptible to out-of-plane buckling.

ACKNOWLEDGEMENTS

The financial support provided by the China Scholarship Council (CSC) for the first author is gratefully acknowledged.

REFERENCES

[1] EN 1993-1-1. Eurocode 3: Design of steel structures - Part 1-1: General rules and rules for buildings. European Committee for Standardization, Brussels, 2005.

[2] L. Gardner, The continuous strength method, Proc. Inst. Civ. Eng. Struct. Build. 161 (2008) 127-133.

[3] D. Butler, G. Anderson, The elastic buckling of tapered beam-columns, Welded Research Supplement 1963, pp. 29-36.

[4] S. Prawel, M. Morell, G. Lee, Bending and buckling strength of tapered structural members, Welding Research Supplement 1974, pp. 75-84.

[5] H. Shiomi, M. Kurata, Strength formula for tapered beam-columns, J. Struct. Eng. 110 (1984) 1630-1643.

[6] M.A. Hirt, M. Crisinel, Charpentes Métaliques-Conception et Dimensionnement des Halles et Bâtiments, Traité de Génie Civil, vol. 11, Press Polytechniques et Universitaires Romandes, Lausanne, 2001.

[7] AISC 360-10, Specifications for Structural Steel Buildings, American Institute of Steel Construction (AISC), Chicago, 2010.

[8] M. Kucukler, L. Gardner, L. Macorini, A stiffness reduction method for the in-plane design of structural steel elements, Eng. Struct. 73 (2014) 72-84.

[9] M. Kucukler, L. Gardner, Design of laterally restrained web-tapered steel structures through a stiffness reduction method, J. Constr. Steel Res. 141 (2018) 63-76.

[10] L. Marques, Tapered steel members: flexural and lateral-torsional buckling, PhD thesis, University of Coimbra, 2012.

[11] L. Marques, A. Taras, L. Simões da Silva, R. Greiner, C. Rebelo, Development of a consistent buckling design procedure for tapered columns, J. Constr. Steel Res. 72 (2012) 61-74.

[12] L. Marques, L. Simões da Silva, R. Greiner, C. Rebelo, A. Taras, Development of a consistent design procedure for lateral-torsional buckling of tapered beams, J. Constr. Steel Res. 89 (2013) 213-235.

[13] L. Marques, L. Simões da Silva, C. Rebelo, A. Santiago, Extension of EC3-1-1 interaction formulae for the stability verification of tapered beam-columns, J. Constr. Steel Res. 100 (2014) 122-135.

[14] T. Tankova, Stability design of steel columns, beams and beam-columns: behaviour, general formulation and reliability, PhD thesis, University of Coimbra, 2018.

[15] T. Tankova, L. Simões da Silva, L. Marques, Buckling resistance of non-uniform steel members based on stress utilization: General formulation, J. Constr. Steel Res. 149 (2018) 239-256.

[16] T. Tankova, J.P. Martins, L. Simões da Silva, R. Simões, H.D. Craveiro, Experimental buckling behaviour of web tapered I-section steel columns, J. Constr. Steel Res. 147 (2018) 293-312.

[17] T. Tankova, J.P. Martins, L. Simões da Silva, L. Marques, H.D. Craveiro, A. Santiago, Experimental lateral-torsional buckling behaviour of web tapered I-section steel beams, Eng. Struct. 168 (2018) 355-370.

[18] J.C. Ermopoulos, Equivalent buckling length of non-uniform members, J. Constr. Steel Res. 42 (2) (1997) 141-158.

[19] I.G. Raftoyiannis, J.C. Ermopoulos, Stability of tapered and stepped steel columns with initial imperfections, Eng. Struct. 27 (2005) 1248-1257.

[20] J. Naumes, Biegeknicken und Biegedrillknicken von Stäben und Stabsystemen auf einheitlicher Grundlage, PhD thesis, RWTH Aachen, Germany, 2009.

[21] L. Simões da Silva, T. Tankova, J.P. Martins, Stability design of steel structures: From members to plates and shells. Proceedings of the International Colloquia on Stability and Ductility of Steel Structures (SDSS 2019), Prague, Czech Republic. CRC Press, 2019.

[22] R.C. Kaehler, D.W. White, Y.D. Kim, Frame design using web-tapered members, American Institute of Steel Construction (AISC) and Metal Building Manufacturers Association (MBMA) Steel Design Guide 25. 2011.

[23] EN 1090-2, Execution of Steel Structures and Aluminium Structures — Part 2: Technical Requirements for Steel Structures, European Committee for Standardization (CEN), Brussels, 2008.

[24] AISC 360-16, Specifications for Structural Steel Buildings, American Institute of Steel Construction (AISC), Chicago, 2016.

[25] EN 1993-1-5. Eurocode 3: Design of steel structures Part 1-5: Plated structural elements. European Committee for Standardization, Brussels, 2006.

[26] L. Gardner, A. Fieber, and L. Macorini, Formulae for calculating elastic local buckling stresses of full structural cross-sections, Structures. 17 (2019) 2-20.

[27] SEMI-COMP, Plastic Member Capacity of Semi-compact Steel Sections — a More Economic Design, European Commission, 2009.

[28] X. Meng, L. Gardner, Simulation and design of semi-compact elliptical hollow sections, Eng. Struct. 202 (2020) 109807.

[29] X. Meng, L. Gardner, A.J. Sadowski, J.M. Rotter, Elasto-plastic behaviour and design of semi-compact circular hollow sections, Thin-Walled Struct. 148 (2020) 106486.

[30] L. Gardner, F. Wang, A. Liew, Influence of strain hardening on the behaviour and design of steel structures, International Journal of Structural Stability and Dynamics. 11 (2011) 855-875.

[31] G.C. Driscoll Jr., L.S. Beedle, The plastic behavior of structural members and frames, Weld. J. 36 (1957) 275-s.

[32] V. Gioncu, D. Petcu, Available rotation capacity of wide-flange beams and beam-columns Part 2. Experimental and numerical tests, J. Constr. Steel Res. 43 (1997) 219-244.

[33] M.G. Lay, T.V. Galambos, The inelastic behavior of beams under moment gradient. Fritz Engineering Laboratory Report No. 297.12, Lehigh University, 1964.

[34] X. Meng, L. Gardner, Cross-sectional behaviour of cold-formed high strength steel circular hollow sections, Thin-Walled Struct. 156 (2020) 106822.

[35] J. Wang, S. Afshan, M. Gkantou, M. Theofanous, C. Baniotopoulos, L. Gardner, Flexural behaviour of hot-finished high strength steel square and rectangular hollow sections, J. Constr. Steel Res. 121 (2016) 97-109.

[36] L. Gardner, N. Saari, F. Wang, Comparative experimental study of hot-rolled and cold-formed rectangular hollow sections, Thin-Walled Struct. 48 (7) (2010) 495-507.

[37] A. Fieber, L. Gardner, L. Macorini, Design of structural steel members by advanced inelastic analysis with strain limits, Eng. Struct. 199 (2019) 109624.

[38] M. Ashraf, L. Gardner, D.A. Nethercot, Structural stainless steel design: Resistance based on deformation capacity, J. Struct. Eng. 134 (2008) 402-411.

[39] S. Afshan, L. Gardner, The continuous strength method for structural stainless steel design, Thin-Walled Struct. 68 (2013) 42-49.

[40] X. Yun, L. Gardner, N. Boissonnade, The continuous strength method for the design of hot-rolled steel cross-sections, Eng. Struct. 157 (2018) 179-191.

[41] X. Yun, L. Gardner, N. Boissonnade, Ultimate capacity of I-sections under combined loading - Part 2: Parametric studies and CSM design, J. Constr. Steel Res. 148 (2018) 265-274.

[42] M. Ashraf, B. Young, Design formulations for non-welded and welded aluminium columns using Continuous Strength Method, Eng. Struct. 33 (2011) 3197-3207.

[43] M.N. Su, B. Young, L. Gardner, Deformation-based design of aluminium alloy beams, Eng. Struct. 80 (2014) 339-349.

[44] M.N. Su, B. Young, L. Gardner, The continuous strength method for the design of aluminium alloy structural elements, Eng. Struct. 122 (2016) 338-348.

[45] A. Fieber, L. Gardner, L. Macorini, Structural steel design using second-order inelastic analysis with strain limits, J. Constr. Steel Res. 168 (2020) 105980.

[46] Z. Li and B. W. Schafer. Buckling analysis of cold-formed steel members with general boundary conditions using CUFSM: Conventional and constrained finite strip methods. In Twentieth International Speciality Conference on Cold-Formed Steel Structures. Saint Louis, Missouri, USA, 2010.

[47] X. Yun, L. Gardner, Stress-strain curves for hot-rolled steels, J. Constr. Steel Res. 133 (2017) 36-46.

[48] A. Fieber, Structural steel design using advanced analysis with strain limits, PhD thesis, Imperial College London, 2019.

[49] A. Fieber, L. Gardner, L. Macorini, Formulae for determining elastic local buckling half-wavelengths of structural steel cross-sections, J. Constr. Steel Res. 159 (2019) 493-506.

[50] ABAQUS. ABAQUS/standard user's manual. Version 6.17. Dassault Systemes Simulia Corp. USA; 2017.

[51] S.L. Chan, S.W. Liu, Y.P. Liu, Second-order direct analysis of steel structures made of tapered members. Proceedings of the 12th International Conference on Advances in Steel-Concrete Composite Structures (ASCCS 2018), University of Politecnica Valencia, Valencia, Spain 2018, p. 75-82.

[52] prEN 1993-1-1. Eurocode 3: Design of steel structures - Part 1-1: General rules and rules for buildings. 2019.

[53] J. Lindner, U. Kuhlmann, F. Jörg, Initial bow imperfections e0 for the verification of Flexural Buckling According to Eurocode 3 Part 1-1 - additional considerations, Steel Constr. 11 (2018) 30-41.

[54] F. Walport, L. Gardner, D.A. Nethercot, Equivalent bow imperfections for use in design by second order inelastic analysis, Structures. 26 (2020) 670-685.

[55] Z. Xing, M. Kucukler, L. Gardner, Local buckling of stainless steel plates in fire, Thin-Walled Struct. 148 (2020) 106570.

[56] M. Kucukler, Z. Xing, L. Gardner, Behaviour and design of stainless steel I-section columns in fire, J. Constr. Steel Res. 165 (2020) 105890.

[57] M. Kucukler, L. Gardner, L. Macorini, Lateral-torsional buckling assessment of steel beams through a stiffness reduction method, J. Constr. Steel Res. 109 (2015) 87-100.

[58] M. Kucukler, L. Gardner, L. Macorini, Flexural-torsional buckling assessment of steel beam-columns through a stiffness reduction method, Eng. Struct. 101 (2015) 662676.

[59] ECCS, Ultimate Limit State Calculation of Sway Frames with Rigid Joints, Tech. Rep.; No. 33, Technical Committee 8 (TC 8) of European Convention for Constructional Steelwork (ECCS). 1984.

[60] M. Kucukler, L. Gardner, Design of web-tapered steel beams against lateral-torsional buckling through a stiffness reduction method, Eng. Struct. 190 (2019) 246-261.

[61] S.P. Prawel, M.L. Morrell, G.C. Lee, Bending and Buckling Strength of Tapered Structural Members., Weld. J. (Miami, Fla). 53 (1974) 75-84.

[62] I.M. Cristutiu, D.L. Nunes, A.I. Dogariu, Experimental study on laterally restrained steel columns with variable I cross-sections, Steel Compos. Struct. 13 (2012) 225-238.

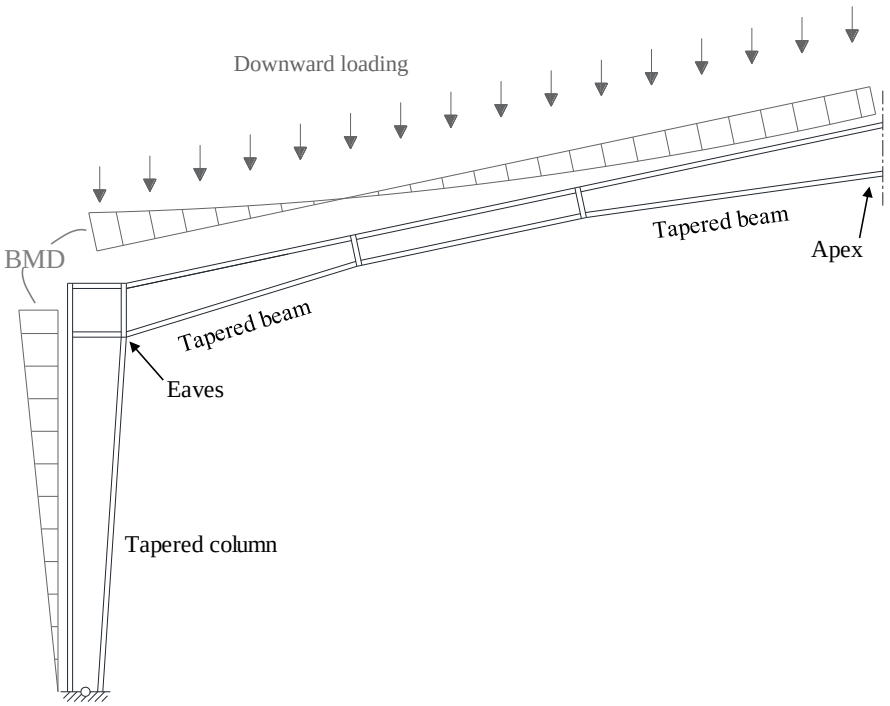

Fig. 1 Downward loading with corresponding bending moment diagram (BMD) on a typical portal frame with tapered beams and tapered columns

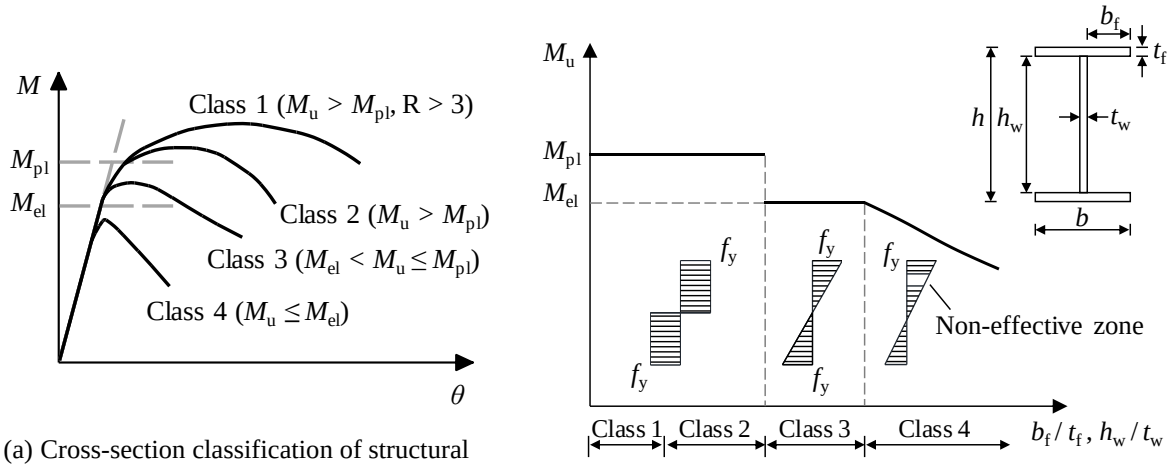

(a) Cross-section classification of structural steel sections in bending

(b) Cross-section bending resistances based on classification

Fig. 2 Cross-section classification and corresponding identical bending resistances according to EN 1993-1-1 [1]

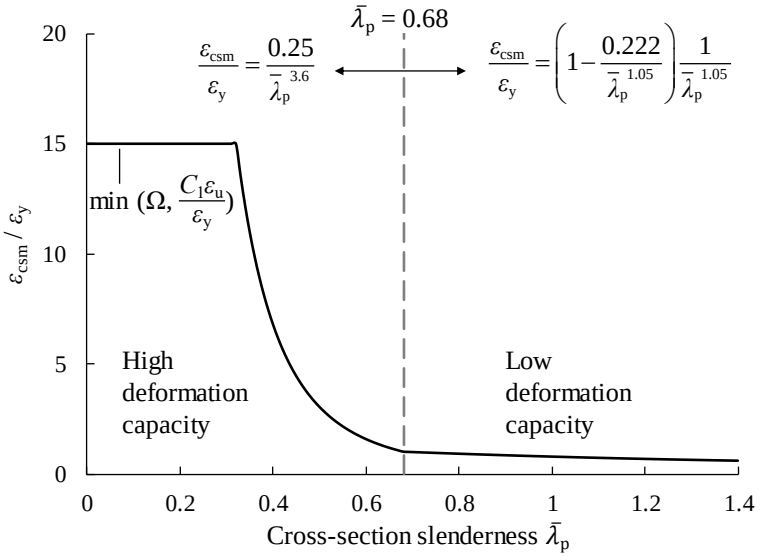

Fig. 3 CSM base curve: a continuous relationship between the cross-section slenderness $\bar{\lambda}_p$ and the deformation capacity expressed by the normalised limiting strain $\varepsilon_{csm}/\varepsilon_y$.

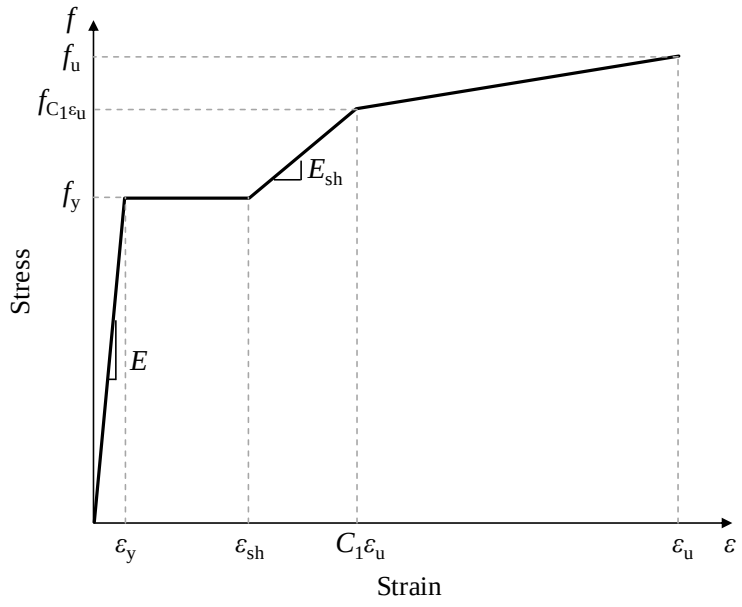

Fig. 4 Quad-linear material model for hot-rolled steel adopted in this study [47]

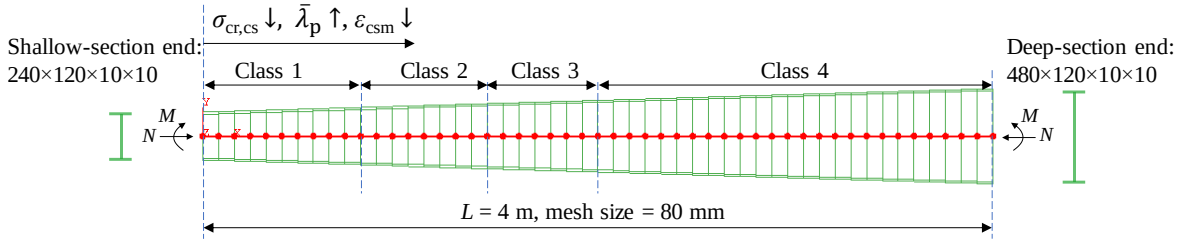

Fig. 5 Variation in cross-section classification along the length of a tapered member under combined axial compression and uniform major axis bending

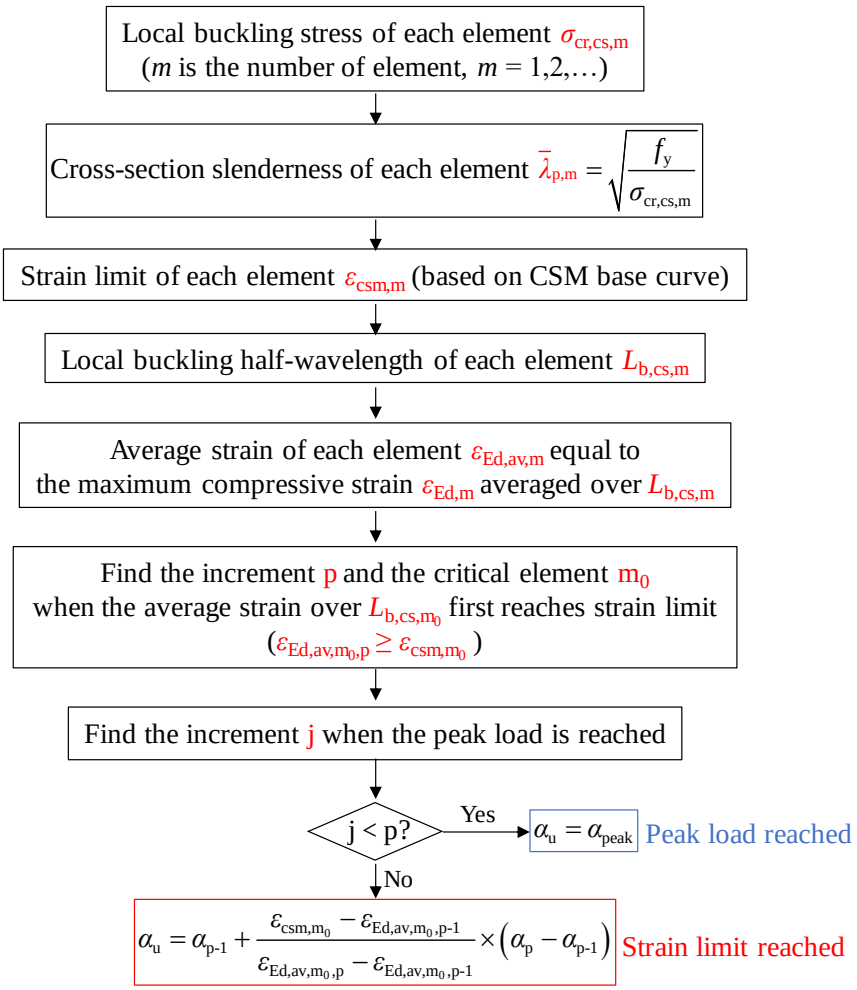

Fig. 6 Process to apply the method of beam element advanced analysis with CSM strain limit to tapered members (where α_u, α_{peak}, and α_p are the predicted ultimate load factor, the peak load factor, and the load factor at increment p respectively)

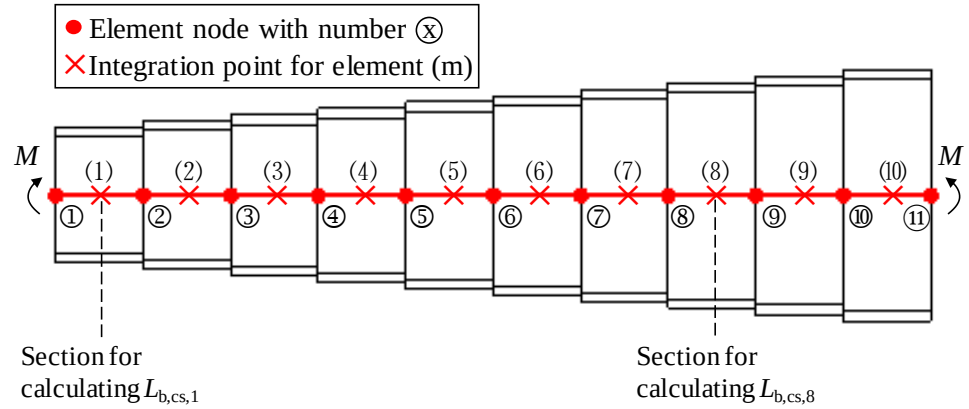

(a) Beam finite element model of a tapered member

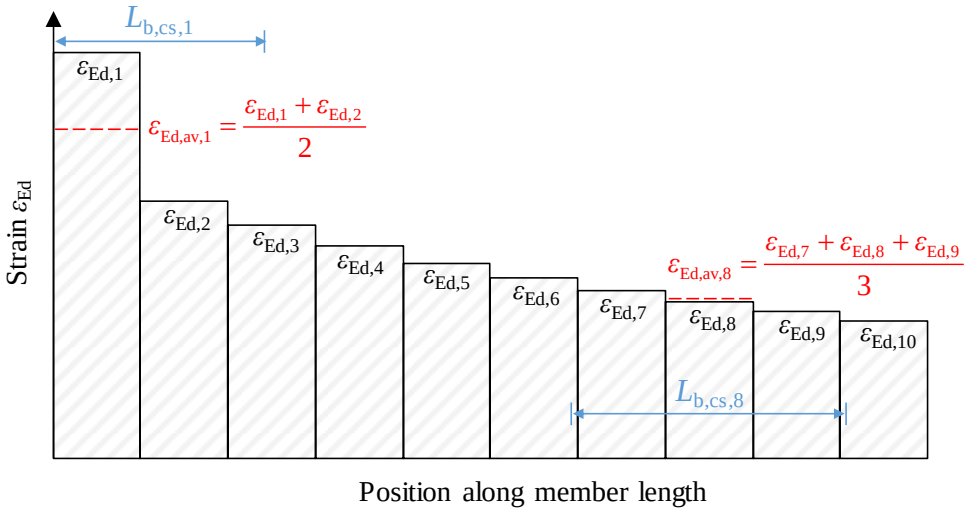

(b) Strain distribution along the member length

Fig. 7 Schematic representation of the strain averaging approach along a member with 10 beam elements; the average strains for elements 1 and 8, $\varepsilon_{Ed,av,1}$ and $\varepsilon_{Ed,av,8}$ respectively, are shown.

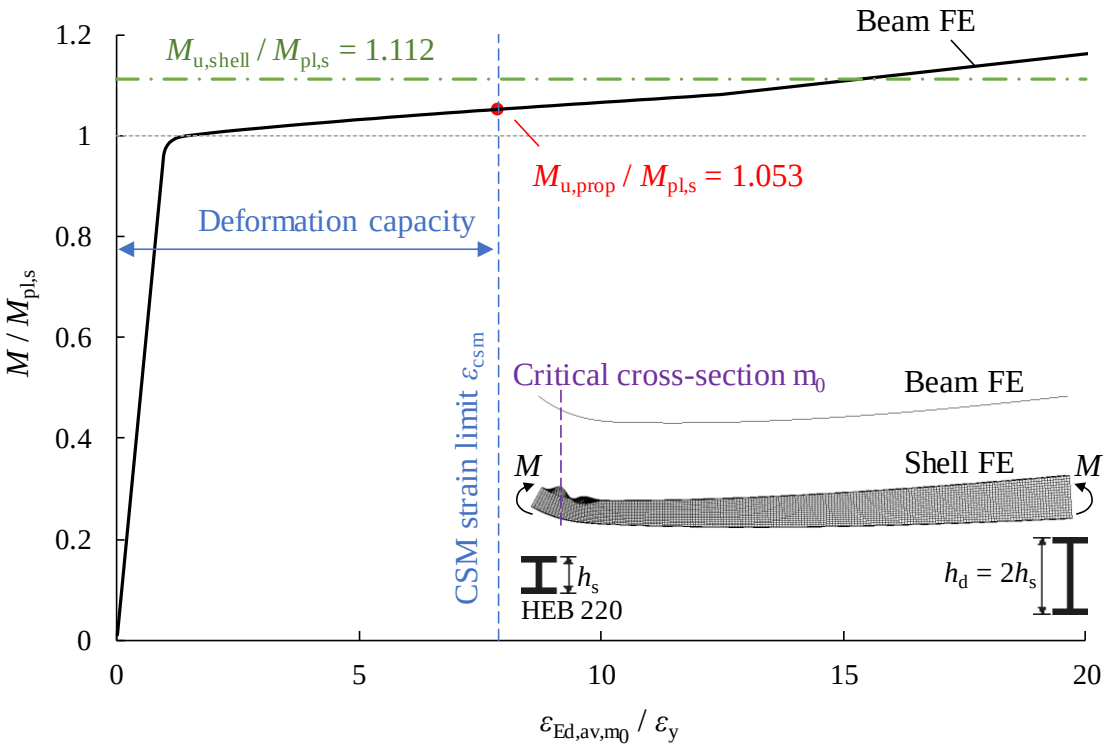

Fig. 8 An illustrative example of the proposed design method using advanced analysis with strain limits on a tapered member under uniform bending (member length L = 5300 mm)

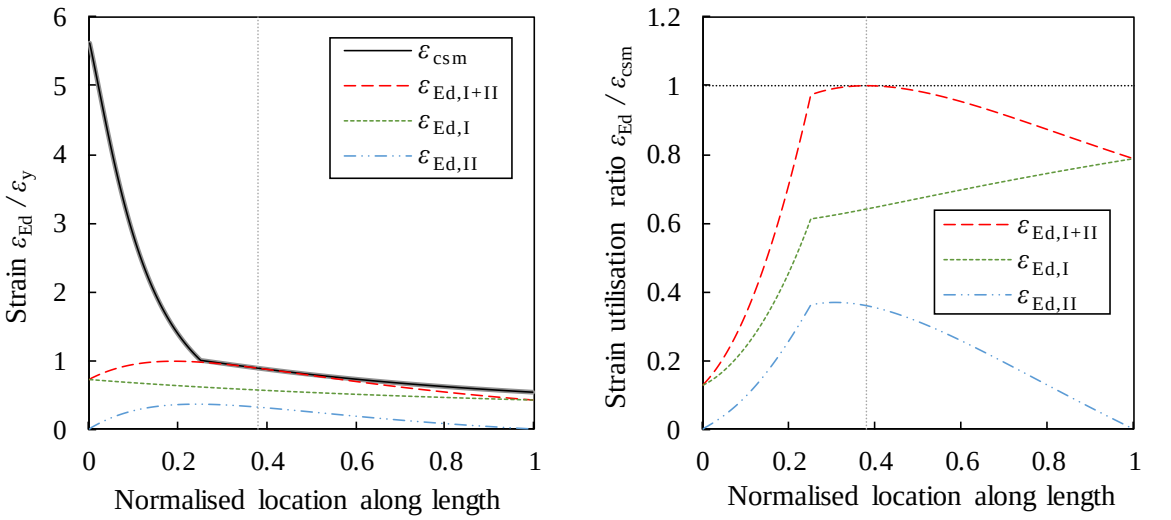

(a) CSM strain limit and strain distribution along member length

(b) Variation of strain utilisation ratio along member length

Fig. 9 (a) CSM strain limit and strain distribution and (b) variation of strain utilisation ratio at the ultimate state (i.e. when $\varepsilon_{Ed,I+II} = \varepsilon_{csm}$) along the length of a tapered column, where the shallow-section end is an HEB 220, the taper ratio γ = 5 and $\bar{\lambda}_y$ = 0.8

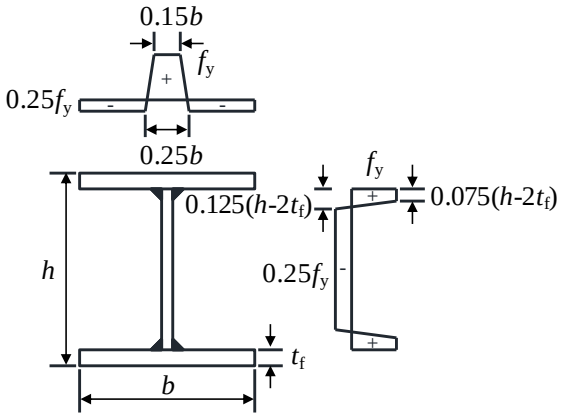

Fig. 10 Residual stress pattern applied to shell finite element models (+ve = tension; -ve = compression)

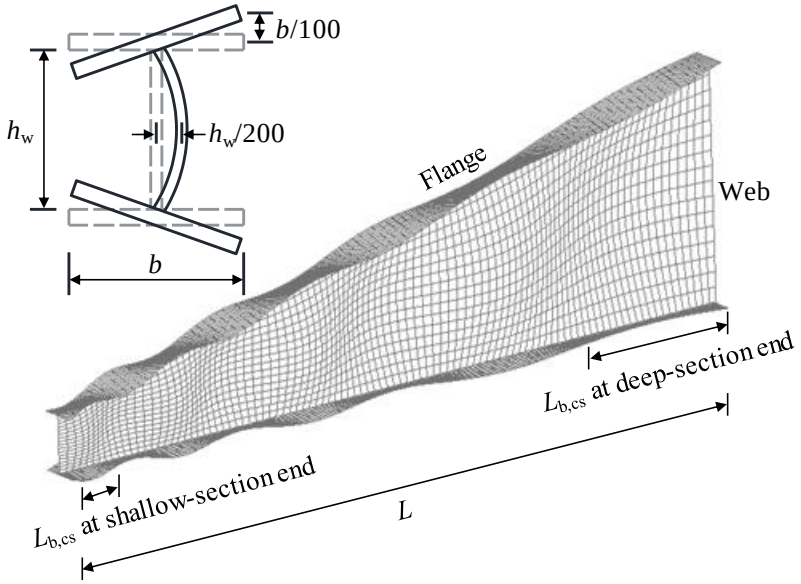

Fig. 11 Definition of local geometric imperfections along the member length

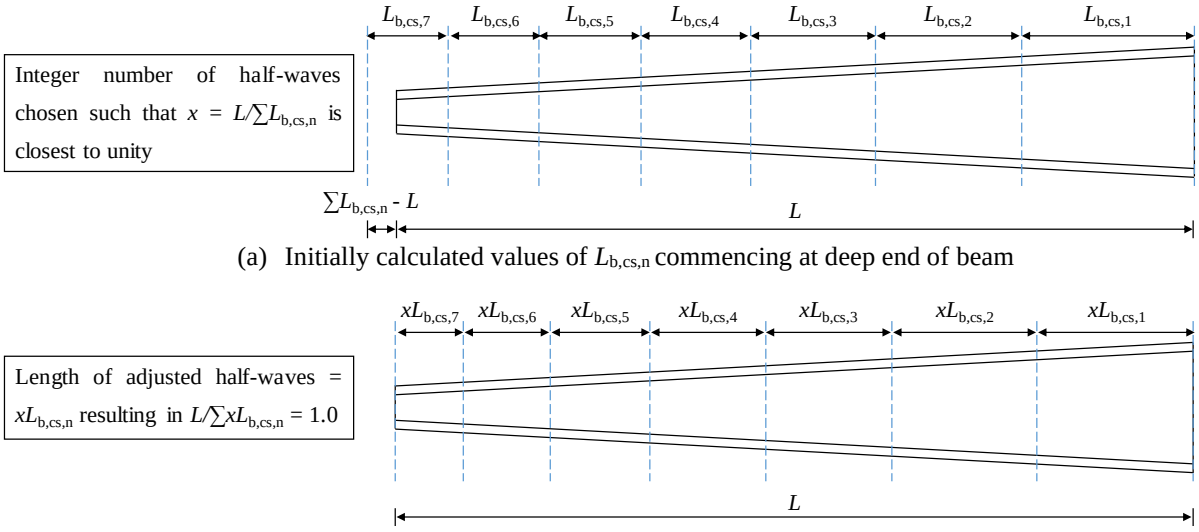

Fig. 12 Illustration of procedure adopted in the application of local imperfections

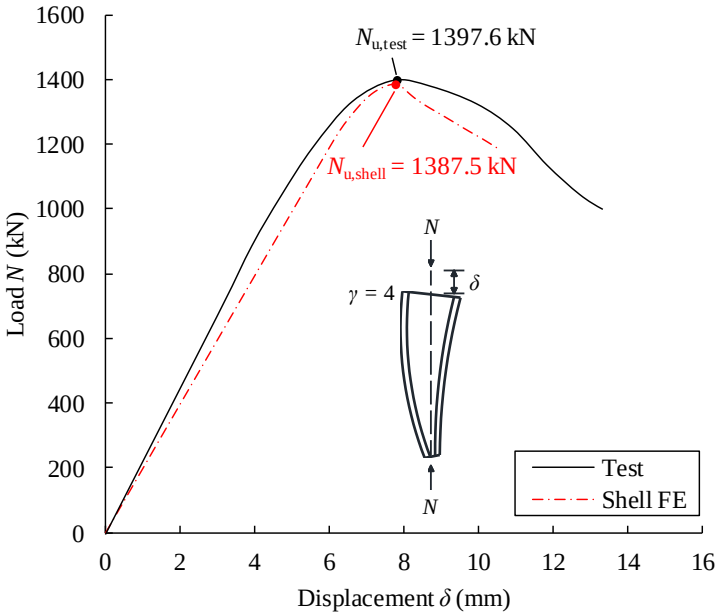

Fig. 13 Comparison of experimental and numerical load-displacement curves of the tapered column specimen C1 tested in [16]

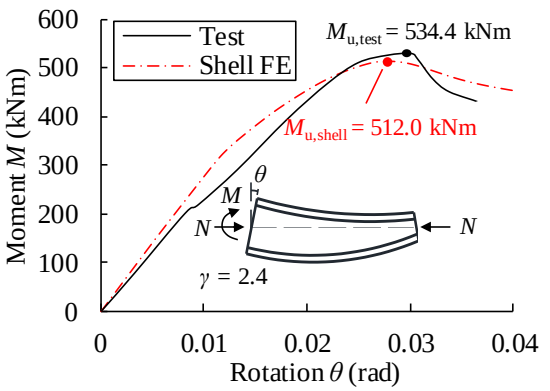

(a) Moment-rotation curve of beam-column specimen C1-8-TR with lateral and torsional restraints

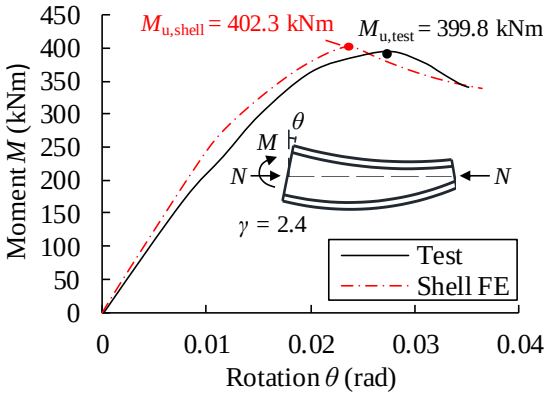

(b) Moment-rotation curve of beam-column specimen C2-6-NR without lateral restraints

Fig. 14 Comparison of experimental and numerical moment-rotation curves of beam-columns tested in [62] (a) specimen C1-8-TR with lateral and torsional restraints; (b) specimen C2-6-NR without lateral restraints.

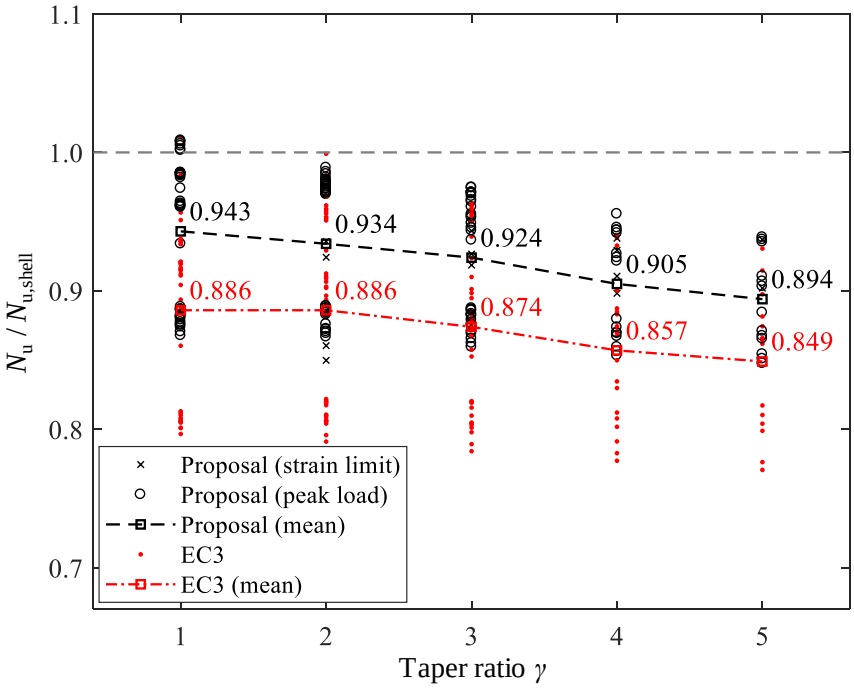

(a) Compression

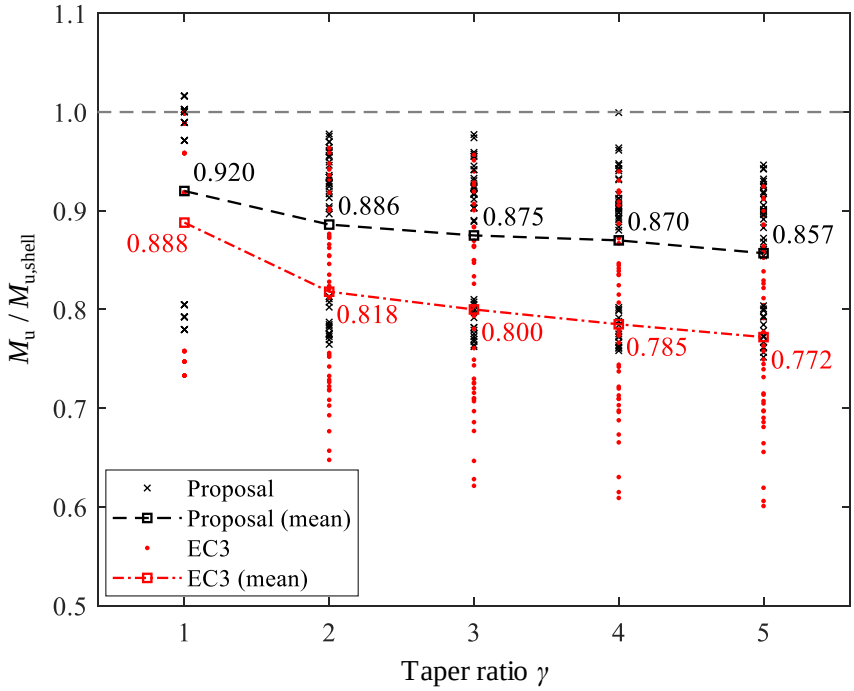

(b) Uniform bending

Fig. 15 Comparison of the ratios of the ultimate load carrying capacities obtained using the proposed design approach and Eurocode 3 to those obtained from the benchmark shell element models versus taper ratio γ for tapered members under (a) axial compression and (b) uniform major axis bending

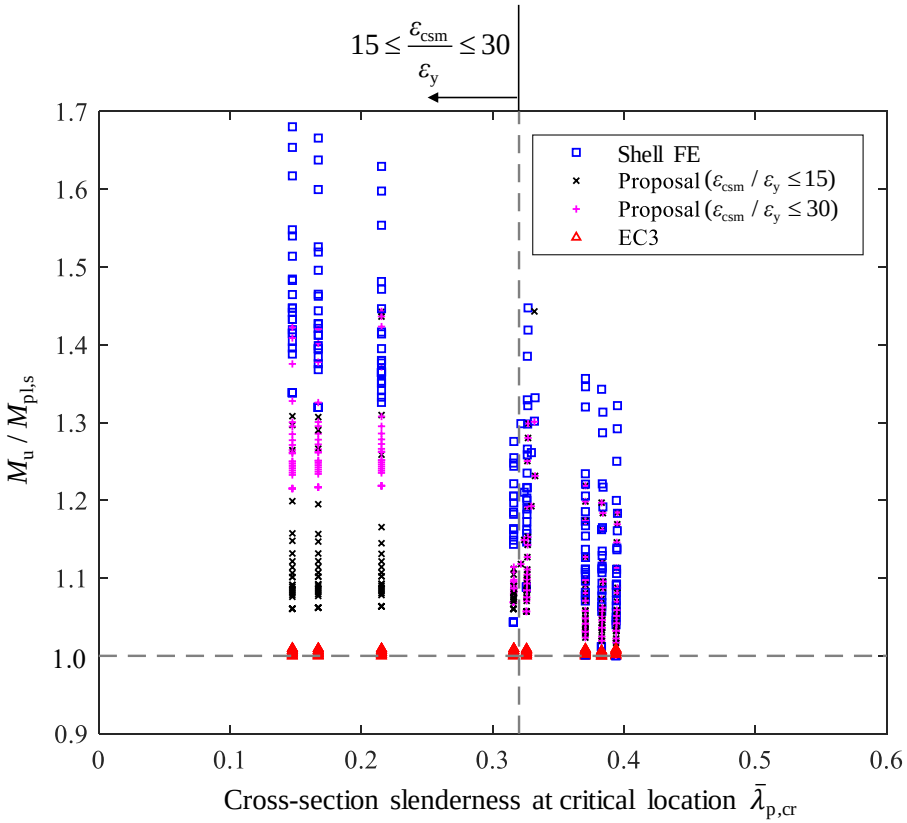

Fig. 16 Comparison of the ratios of the ultimate capacities obtained from shell FE, the proposed design approach and Eurocode 3 to that corresponding to the attainment of the plastic moment at the shallow end cross-section $M_u/M_{pl,s}$ versus cross-section slenderness at the critical location $\bar{\lambda}_{p,cr}$ for tapered members under uniform bending; all tapered beams are governed by the CSM strain limit, rather than peak load

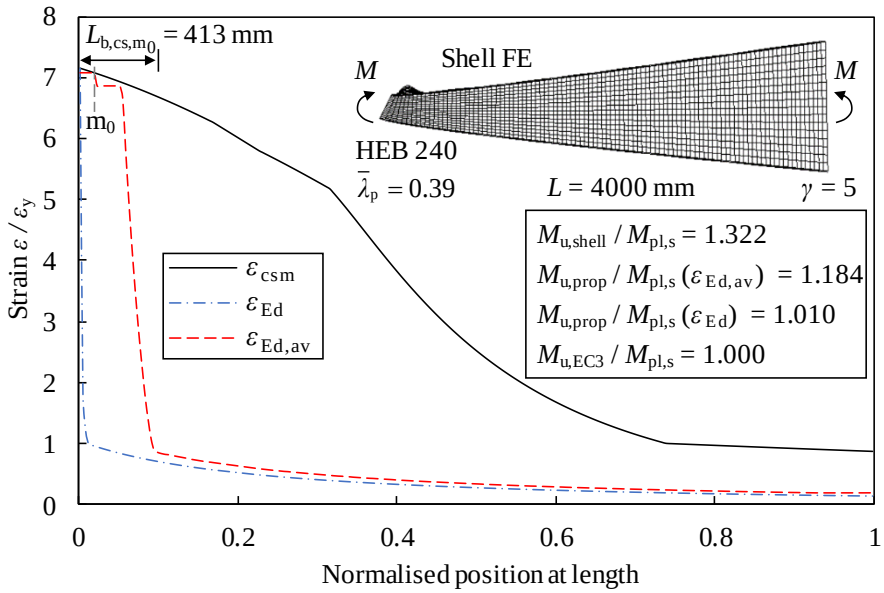

Fig. 17 Variation of CSM strain limit ε_{csm}, maximum longitudinal compressive strain ε_{Ed} (for the load level at which $\varepsilon_{Ed} = \varepsilon_{csm}$) and average maximum longitudinal compressive strain $\varepsilon_{Ed,av}$ (for the load level at which $\varepsilon_{Ed,av} = \varepsilon_{csm}$), along the length of a tapered member under uniform bending. The critical element m_0 when strain averaging is considered (i.e. that in which $\varepsilon_{Ed,av}$ first reaches ε_{csm}, signifying failure) is close to the shallow end of the beam, mirroring the failure location indicated by the benchmark shell FE model. The local buckling half-wavelength for the cross-section at this location L_{b,cs,m_0} = 413 mm. The average strain for the critical element ε_{Ed,av,m_0} is obtained by averaging the maximum longitudinal compressive strains for all elements (of which there are 28 in the present example) that lie entirely within L_{b,cs,m_0}, as illustrated in Fig. 7.

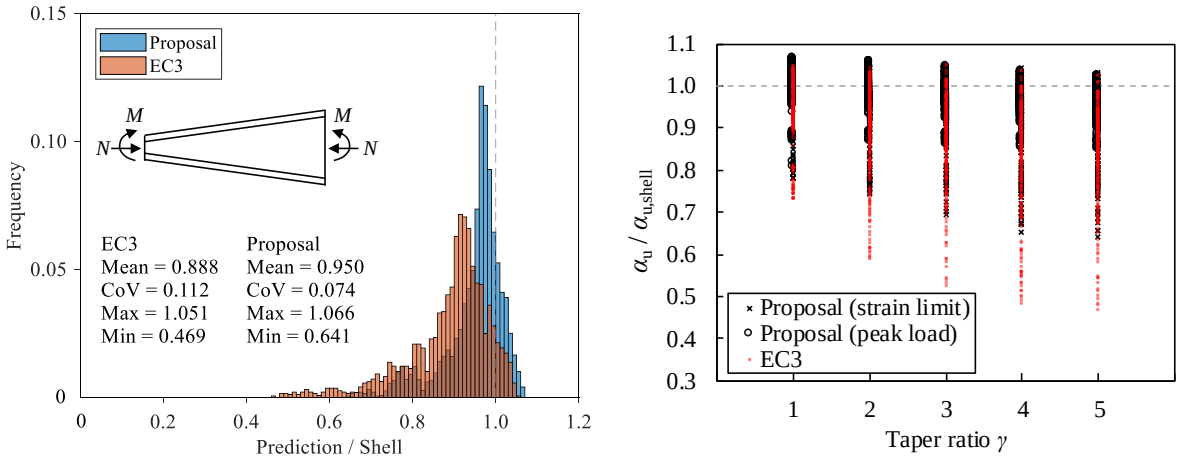

(a) Frequency distributions (b) Ultimate capacities versus taper ratio

Fig. 18 Comparison between the ratios of the ultimate capacities predicted by the proposed design method and Eurocode 3 to those obtained from benchmark shell finite element models $\alpha_u/\alpha_{u,shell}$ for tapered members under uniform bending plus axial compression

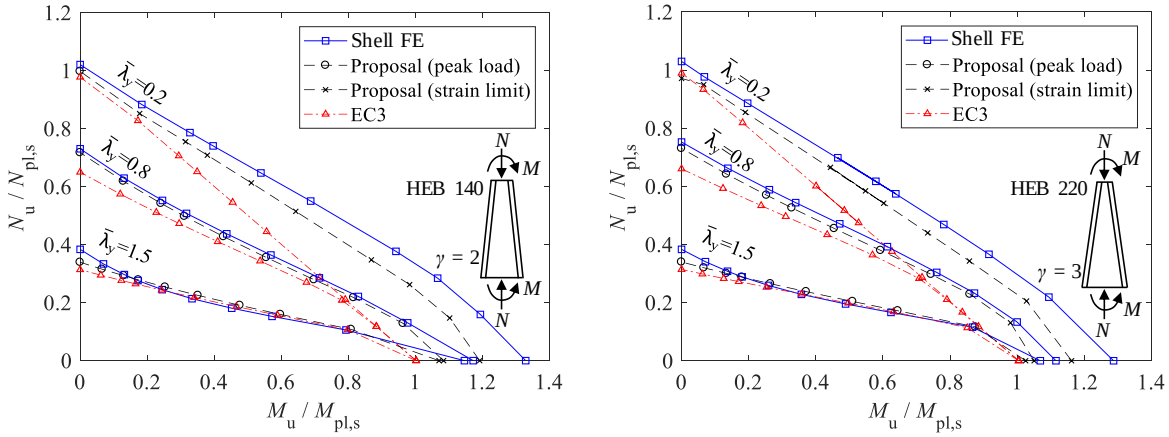

(a) HEB 140, $\gamma = 2$ (b) HEB 220, $\gamma = 3$

Fig. 19 Comparison of the ultimate strengths determined using the proposed design approach against benchmark shell element models and Eurocode 3 for tapered members with different member slendernesses under axial compression and uniform major axis bending

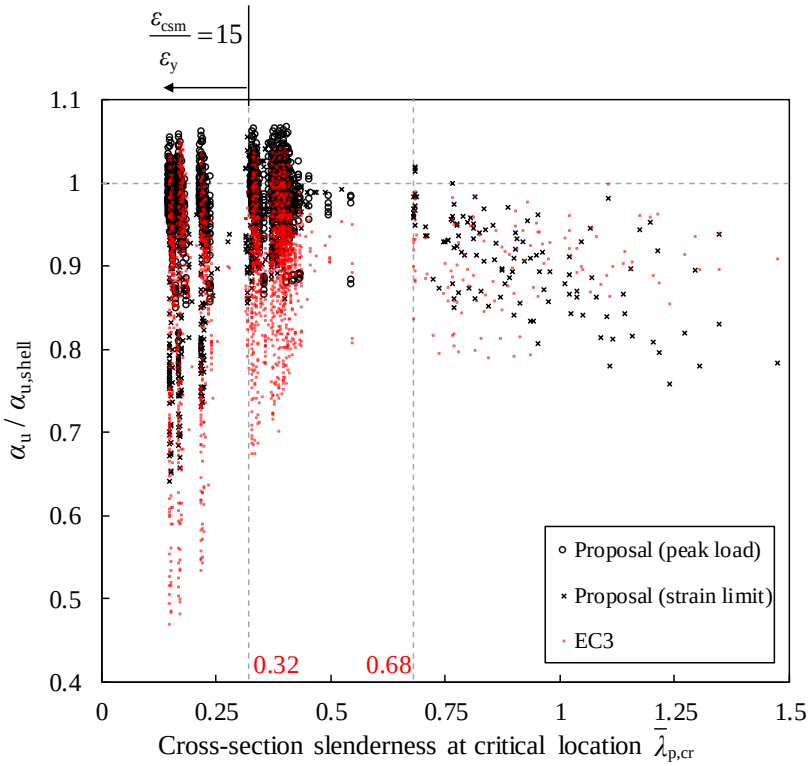

Fig. 20 Comparison of the ratios of the ultimate capacities obtained from proposed design approach and Eurocode 3 to those obtained from benchmark shell finite element models $\alpha_u/\alpha_{u,shell}$ versus cross-section slenderness at the critical location $\bar{\lambda}_{p,cr}$ for tapered members under combined compression and uniform major axis bending

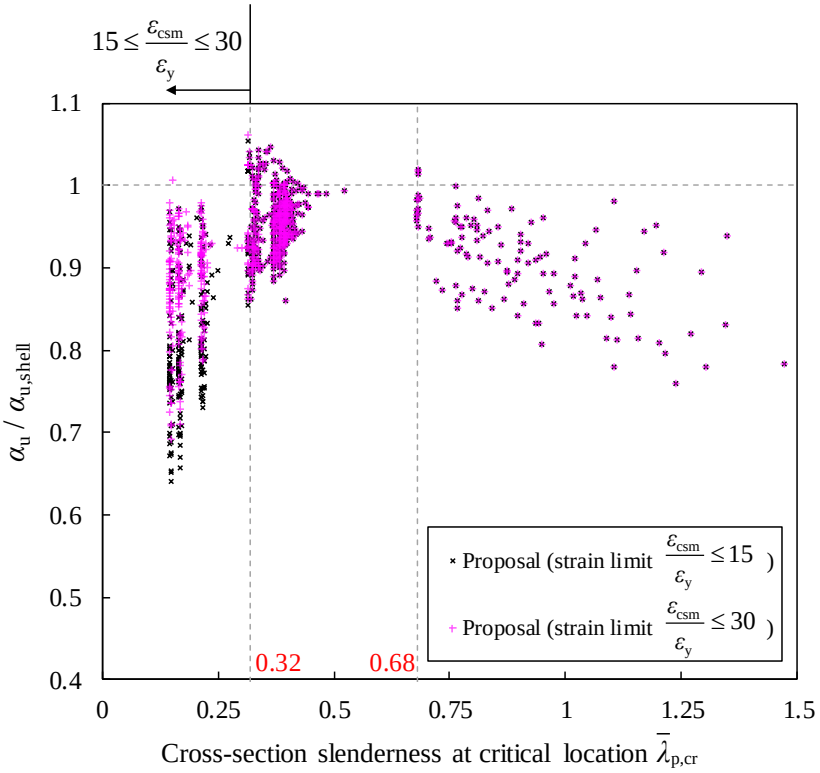

Fig. 21 Ratios of the ultimate load carrying capacities predicted by the proposed design method using $15\varepsilon_y$ or $30\varepsilon_y$ as the maximum strain limit to those determined from the benchmark shell finite element models $\alpha_u/\alpha_{u,shell}$ for tapered members under combined compression and uniform major axis bending, considering only cases when the strain limit, rather than the peak load, governed.

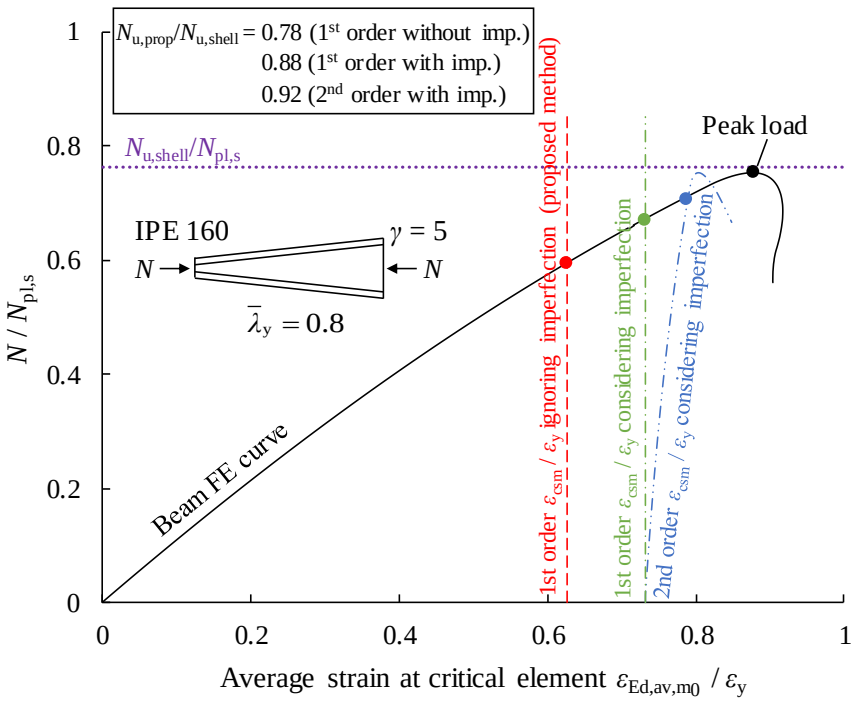

Fig. 22 An illustrative example to show the difference between the ultimate member resistances predicted by the proposed design method using strain limits determined based on first order or second order internal force / moment distributions

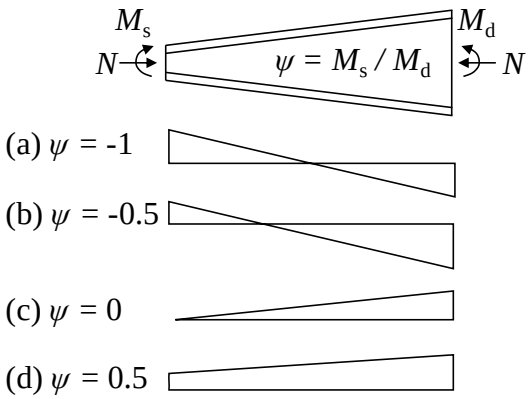

Fig. 23 Load cases considered for tapered members under combined compression and non-uniform bending along the member length

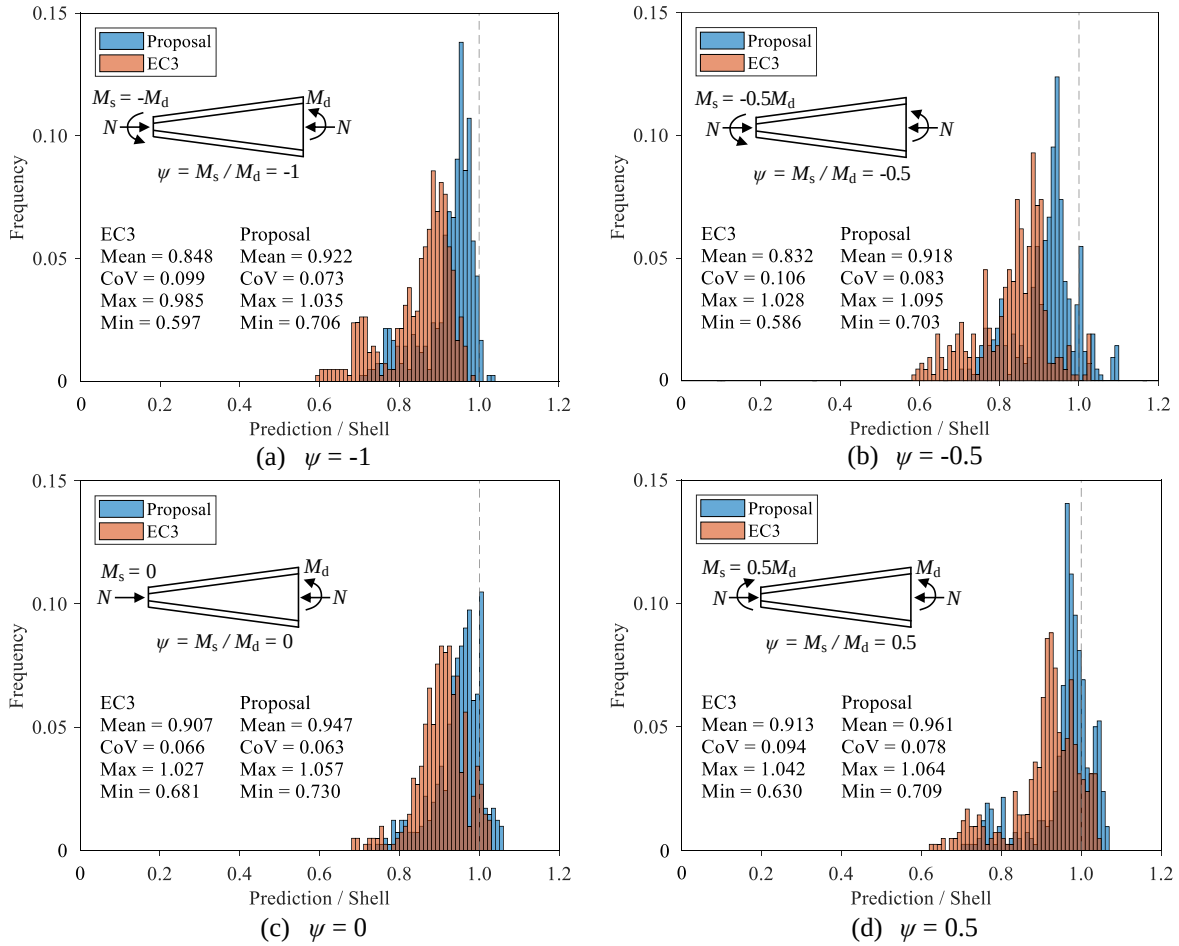

Fig. 24 Frequency distributions of the ratios of the ultimate capacities predicted using the proposed design method and Eurocode 3 to those obtained from the benchmark shell finite element models $\alpha_u/\alpha_{u,shell}$ for tapered members under combined compression and non-uniform bending

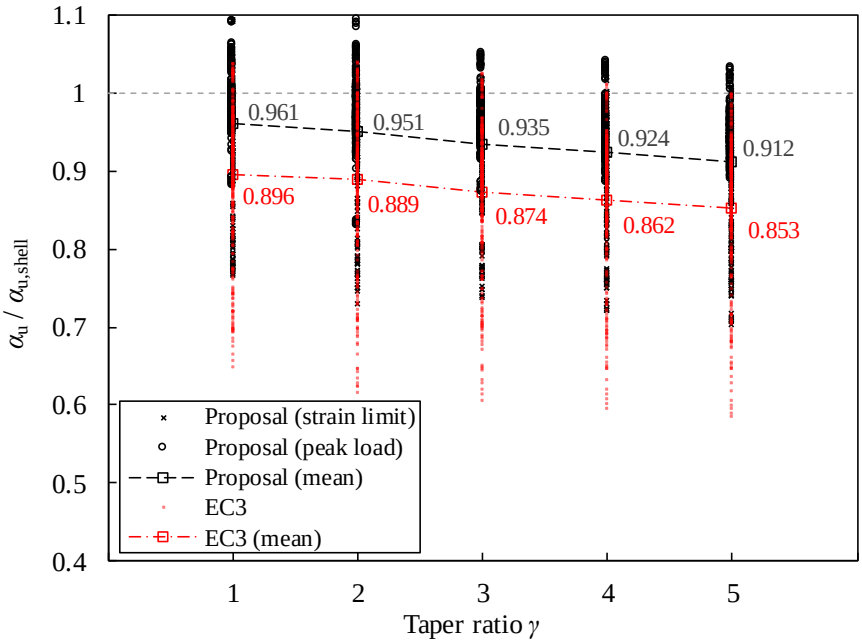

Fig. 25 Comparison between the ratios of the ultimate load carrying capacities predicted using the proposed design method and Eurocode 3 to those determined from the benchmark shell finite element models versus taper ratio γ for tapered members under combined compression and non-uniform bending

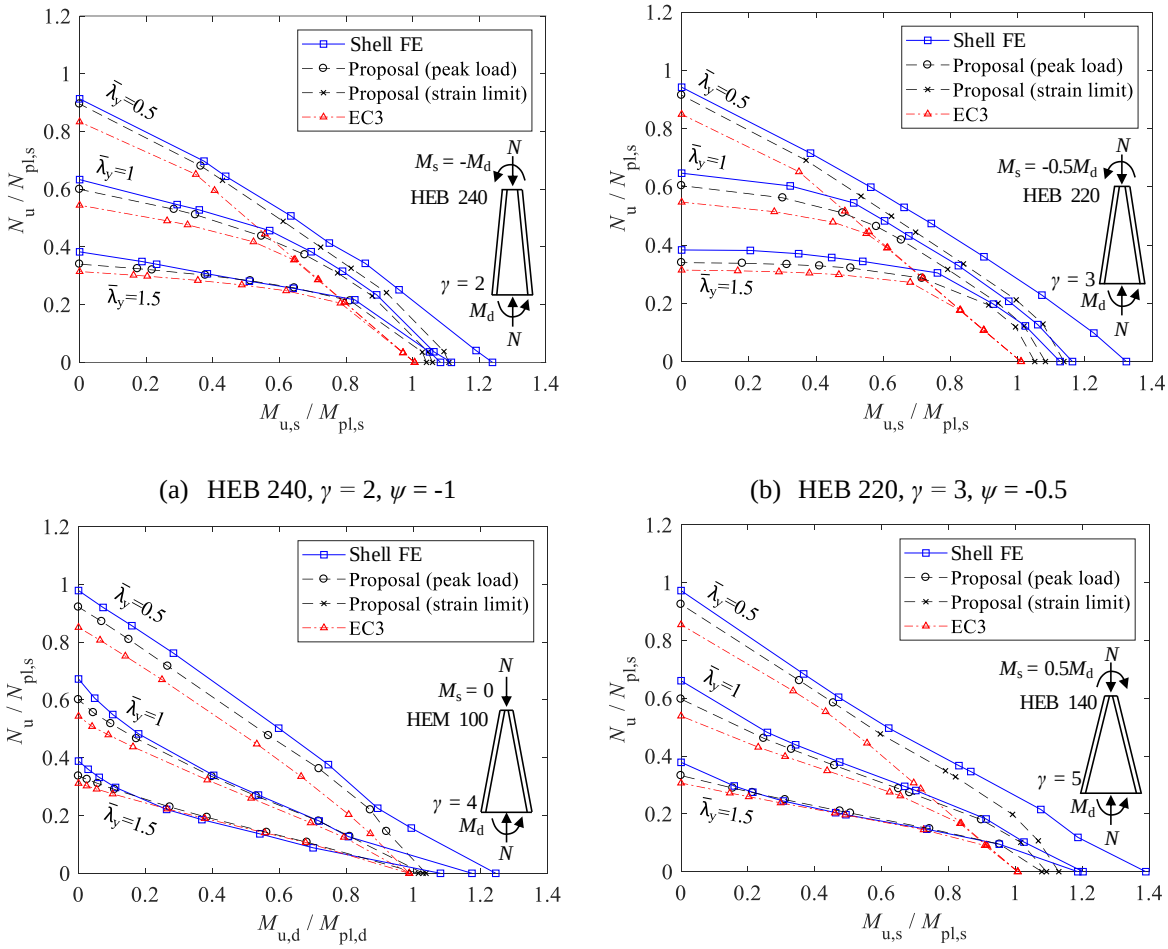

(a) HEB 240, γ = 2, ψ = -1

(b) HEB 220, γ = 3, ψ = -0.5

(c) HEM 100, γ = 4, ψ = 0

(d) HEB 140, γ = 5, ψ = 0.5

Fig. 26 Comparison of the ultimate strengths determined using the proposed design approach with the benchmark shell finite element models and Eurocode 3 for tapered members with different member slendernesses under axial compression and non-uniform major axis bending

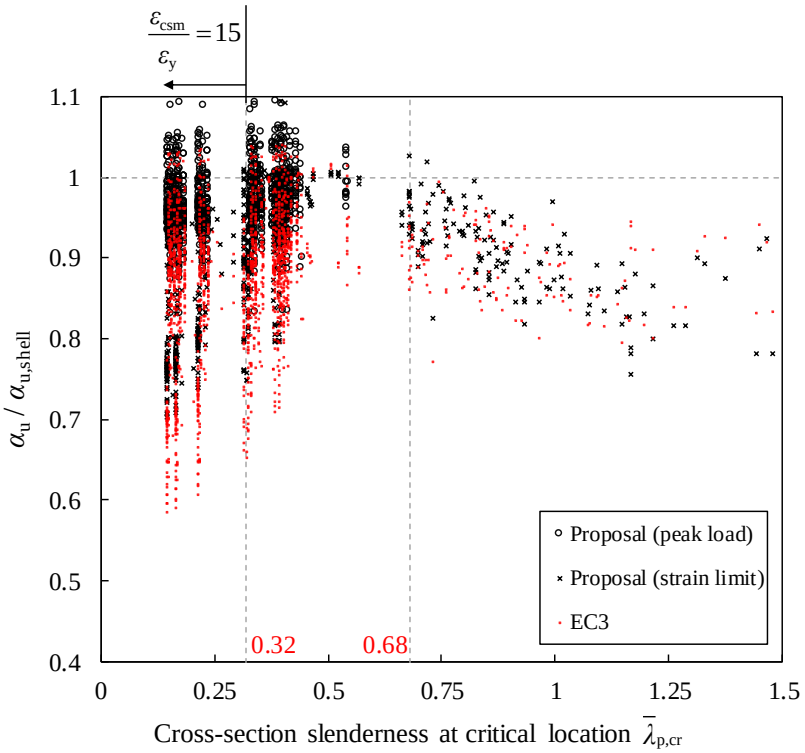

Fig. 27 Comparison of the ratios of the ultimate load carrying capacities obtained using the proposed design approach and Eurocode 3 to those obtained from the benchmark shell finite element models $\alpha_u/\alpha_{u,shell}$ versus cross-section slenderness at the critical location $\bar{\lambda}_{p,cr}$ for tapered members under combined compression and non-uniform bending

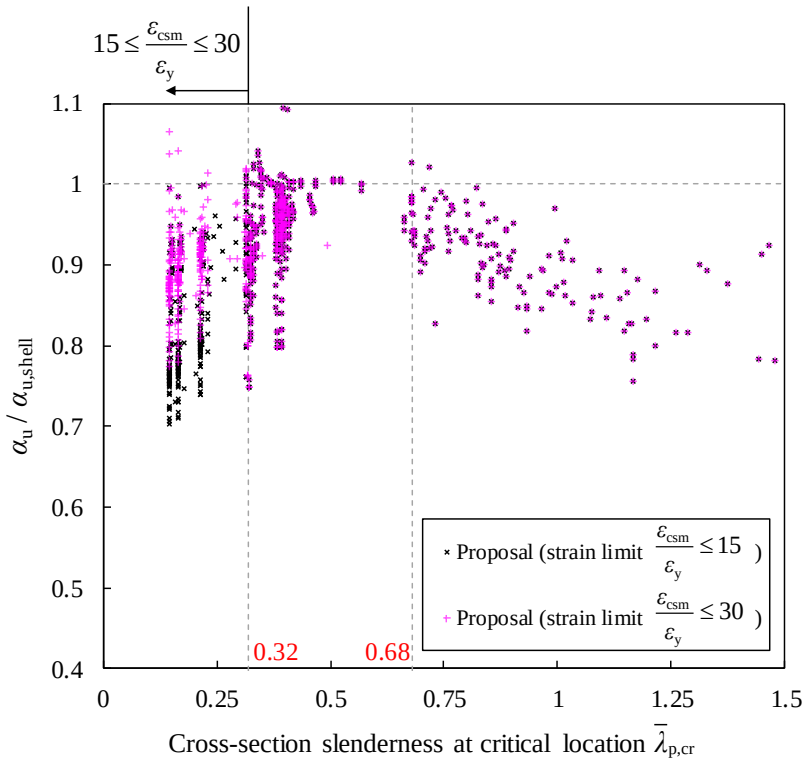

Fig. 28 Ratios of ultimate load carrying capacities predicted using the proposed design method using $15\varepsilon_y$ or $30\varepsilon_y$ as the maximum strain limit to those obtained from the benchmark shell finite element models $\alpha_u/\alpha_{u,shell}$ for tapered members under non-uniform bending, considering only cases when the strain limit, rather than the peak load, governed.

Table 1 Summary of validation of shell finite element models, and comparison of results obtained from the proposed design method and Eurocode 3 relative to experimental results. LR = lateral restraints; NR = no restraints; TR = lateral and torsional restraints. The ultimate load factors obtained from the tests, shell FE modelling, proposed design method and Eurocode 3 are denoted $\alpha_{u,test}$, $\alpha_{u,shell}$, $\alpha_{u,prop}$ and $\alpha_{u,EC3}$, respectively.

Reference	Test	Member shape	Member type	Taper ratio γ	Material	Lateral restraints	$\alpha_{u,shell}/\alpha_{u,test}$	$\alpha_{u,prop}/\alpha_{u,test}$	$\alpha_{u,EC3}/\alpha_{u,test}$
Tankova et al. (2018) [16]	C1	V	Column	4	S355	LR	0.993	0.862	0.779
	C2	V	Column	2			0.945	0.830	0.829
	C3	L	Column	3			0.974	0.859	0.781
	BC	L	Beam-column	3			0.990	*	*
Prawel et al. (1974) [61]	LB-3	L	Beam	2.67	ASTM A242	LR	0.982	*	*
	LB-5						0.937	0.816	0.804
	LB-6						1.012	*	*
Shiomi & Kurata (1984) [5]	IT-1.4-1	V	Beam-column	1.36	SS-41	LR	1.024	0.760	0.698
	IT-1.6-2			1.50			1.013	0.756	0.688
	IT-1.8-3			1.76			0.998	0.734	0.634
	IT-2.2-5			2.15			1.103	0.811	0.702
	IT-2.4-6			2.30			1.040	0.775	0.678
Cristutiu et al. (2012) [62]	C1-8-NR	L	Beam-column	2.4	S355	NR	0.981	*	*
	C1-8-LR					LR	1.015	*	*
	C1-8-TR					TR	0.958	0.904	0.803
	C2-6-NR					NR	1.017	*	*
	C2-6-LR					LR	1.038	*	*
	C2-6-TR					TR	1.029	0.934	0.910
Mean							1.003	0.822	0.755
CoV							0.039	0.077	0.108
Max							1.103	0.934	0.910
Min							0.937	0.734	0.634
Total number of tests							18	11	11

*Test specimens exhibited large out-of-plane deformations and are therefore outside the scope of the in-plane design methods examined in the present study

Table 2 Summary of varied parameters considered and accuracy of the proposed design method and Eurocode 3 in comparison to the results from benchmark shell FE models for tapered members under axial compression, uniform bending, and combined of compression and uniform bending

Loading condition	Member slenderness $\bar{\lambda}_y$	Taper ratio γ	Shallow-end cross-section	No. of cases N	Design method	$\alpha_u/\alpha_{u,shell}$			
						Mean	CoV	Max	Min
Compression	0.2, 0.5, 0.8, 1.2, 1.5	1, 2, 3, 4, 5	HEM 100, HEM 120, HEB 140, IPE 160, HEM 180, HEB 200, HEB 220, HEB 240	200	Proposed	0.926	0.052	1.009	0.848
					EC3	0.875	0.068	1.011	0.771
Bending				200	Proposed	0.881	0.092	1.016	0.752
					EC3	0.813	0.130	1.000	0.601
Compression + bending				2000	Proposed	0.950	0.074	1.066	0.641
					EC3	0.888	0.112	1.051	0.469

Table 3 Summary of varied parameters considered and accuracy of the proposed design method and Eurocode 3 in comparison to the results from benchmark shell FE models for tapered members under non-uniform bending with or without axial compression

Moment ratio ψ	Member slenderness $\bar{\lambda}_y$	Taper ratio γ	Shallow-end cross-section	No. of cases N	Design method	$\alpha_u/\alpha_{u,shell}$			
						Mean	CoV	Max	Min
-1	0.5, 1.0, 1.5	1, 2, 3, 4, 5	HEM 100, HEM 120, HEB 140, IPE 160, HEM 180, HEB 220, HEB 240	420	Proposed	0.922	0.073	1.035	0.706
					EC3	0.848	0.099	0.985	0.597
-0.5				420	Proposed	0.918	0.083	1.095	0.703
					EC3	0.832	0.106	1.028	0.586
0				420	Proposed	0.947	0.063	1.057	0.730
					EC3	0.907	0.066	1.027	0.681
0.5				420	Proposed	0.961	0.078	1.064	0.709
					EC3	0.913	0.094	1.042	0.630
Total				1680	Proposed	0.937	0.077	1.095	0.703
					EC3	0.875	0.101	1.042	0.586